Author Manuscript

Author Manuscript

Author Manuscript

Author Manuscript

HHS Public Access

Author manuscript

Cell Rep. Author manuscript; available in PMC 2021 April 25.

Published in final edited form as:

Cell Rep. 2020 September 15; 32(11): 108147. doi:10.1016/j.celrep.2020.108147.

PRC2 Acts as a Critical Timer That Drives Oligodendrocyte Fate over Astrocyte Identity by Repressing the Notch Pathway

Wenxian Wang[1], **Hyeyoung Cho**[3], **Dongkyeong Kim**[2], **Younjung Park**[1], **Ji Hwan Moon**[1], **Su Jeong Lim**[6], **Sung Min Yoon**[6], **Michael McCane**[4], **Sue A. Aicher**[5], **Sangsoo Kim**[6], **Ben Emery**[4], **Jae W. Lee**[1], **Seunghee Lee**[7], **Yungki Park**[2], **Soo-Kyung Lee**[1,8,*]

[1]Department of Biological Sciences, College of Arts and Sciences, University at Buffalo, The State University of New York, Buffalo, NY 14260, USA

[2]Hunter James Kelly Research Institute, Department of Biochemistry, Jacobs School of Medicine and Biomedical Sciences, State University of New York at Buffalo, Buffalo, NY 14203, USA

[3]Computational Biology Program, School of Medicine, Oregon Health & Science University, Portland, OR 97239, USA

[4]Jungers Center for Neurosciences Research, Department of Neurology, School of Medicine, Oregon Health & Science University, Portland, OR 97239, USA

[5]Department of Physiology and Pharmacology, School of Medicine, Oregon Health & Science University, Portland, OR 97239, USA

[6]Department of Bioinformatics and Life Science, Soongsil University, Seoul, Korea

[7]College of Pharmacy and Research Institute of Pharmaceutical Sciences, Seoul National University, Seoul 08826, Korea

[8]Lead Contact

SUMMARY

PRC2 creates the repressive mark histone H3 Lys27 trimethylation. Although PRC2 is involved in various biological processes, its role in glial development remains ambiguous. Here, we show that PRC2 is required for oligodendrocyte (OL) differentiation and myelination, but not for OL precursor formation. PRC2-deficient OL lineage cells differentiate into OL precursors, but they fail to trigger the molecular program for myelination, highlighting that PRC2 is essential for directing the differentiation timing of OL precursors. PRC2 null OL lineage cells aberrantly

This is an open access article under the CC BY-NC-ND license (http://creativecommons.org/licenses/by-nc-nd/4.0/).

*Correspondence: slee229@buffalo.edu.

AUTHOR CONTRIBUTIONS

Conceptualization, W.W. and S.-K.L.; Methodology, W.W., D.K., Younjung P., S.A.A., B.E., S.L., Yungki P., and S.-K.L.; Investigation, W.W. and S.-K.L.; Formal Analysis, W.W., H.C., J.H.M., S.J.L., S.M.Y., and S.K.; Writing – Original Draft, W.W. and S.-K.L.; Writing – Review & Editing, W.W., J.W.L., and S.-K.L.; Supervision, J.W.L. and S.-K.L.; Funding Acquisition, S.A.A., S.K., B.E., S.L., Yungki P., J.W.L., and S.-K.L.

DECLARATION OF INTERESTS

The authors declare no competing interests.

SUPPLEMENTAL INFORMATION

Supplemental Information can be found online at https://doi.org/10.1016/j.celrep.2020.108147.

Author Manuscript Author Manuscript Author Manuscript Author Manuscript

induce Notch pathway genes and acquire astrocytic features. The repression of the Notch pathway restores the myelination program and inhibits abnormal astrocytic differentiation in the PRC2-deficient OL lineage, indicating that Notch is a major target of PRC2. Altogether, our studies propose a specific action of PRC2 as a novel gatekeeper that determines the glial fate choice and the timing of OL lineage progression and myelination by impinging on the Notch pathway.

In Brief

Wang et al. show that the polycomb repressive complex PRC2 is required for the differentiation of oligodendrocyte precursors to myelinating oligodendrocytes. They further show that PRC2 promotes oligodendrocyte differentiation and inhibits erroneous astrocytic fate by repressing the Notch pathway.

Graphical Abstract

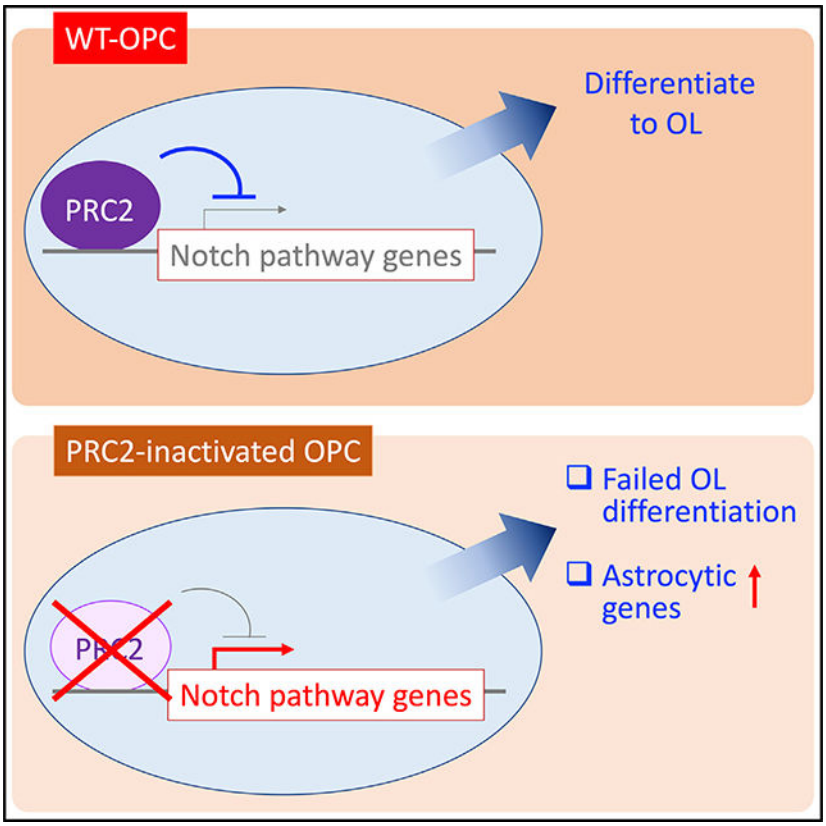

INTRODUCTION

The central nervous system (CNS) is composed of enormously divergent types of neurons and glia, which emerge from neural progenitor cells in a stereotypic order during development. Epigenetic regulation, such as post-translational modification of nucleosomal histones, plays an important role in cell differentiation and cell fate determination (Chen and Dent, 2014). The polycomb repressive complex PRC2 is the histone methyltransferase complex that regulates chromatin conformation and gene expression via deposition of

Author Manuscript Author Manuscript Author Manuscript Author Manuscript

trimethylation at the histone H3 lysine 27 residue (H3K27me3) (Margueron and Reinberg, 2011). H3K27me3 is a highly dynamic histone mark associated with transcriptionally repressive chromatin. PRC2 consists of four core subunits: RBBP7/4, Suz12, Eed, and either the Ezh2 or the Ezh1 enzyme that catalyzes H3K27me3 (Margueron and Reinberg, 2011). In the developing cortex, Ezh2 plays a role in neural progenitor cells but is downregulated in neurons and astrocytes (Hirabayashi et al., 2009; Pereira et al., 2010). Although Ezh2 is considered a dominant enzyme in PRC2, Ezh1 also exhibits H3K27 methyltransferase activity and functions redundantly with Ezh2 in the hair follicle and mammary alveoli (Ezhkova et al., 2011; Yoo et al., 2015). PRC2 is known to regulate developmental genes in stem/progenitor cells (Margueron and Reinberg, 2011), but the *in vivo* actions of PRC2 in neuro-glial fate decisions and lineage progression have not been fully elucidated.

Oligodendrocytes (OLs) and astrocytes are the two main types of glia. OLs are responsible for myelination of axons in the CNS and critical for brain function and homeostasis. The stepwise differentiation of OLs is controlled temporally and spatially during development (Emery and Lu, 2015). In the developing spinal cord, most OLs are derived from a progenitor domain in the ventricular zone, named the progenitors for motor neuron (pMN) domain (Lu et al., 2000; Zhou et al., 2000). The progenitors in the pMN domain produce spinal motor neurons initially and then switch to generate OL precursor cells (OPCs), which migrate from the ventricular zone to the lateral area (Lu et al., 2002; Takebayashi et al., 2002; Zhou and Anderson, 2002). OPCs proliferate and then differentiate into OLs that express myelin genes. Notably, OPCs can adopt an astrocytic fate under certain conditions (Kondo and Raff, 2000b; Nunes et al., 2003; Zhu et al., 2012), suggesting that OPCs possess the plasticity to adopt such a fate. Developmental signaling pathways Notch and Wnt play spatiotemporally specific roles in the commitment of glial progenitors and the progression of OL lineage during development (He and Lu, 2013). In addition, a series of epigenetic regulators and transcription factors have been identified to control the differentiation of the OL lineage cells (Emery and Lu, 2015). These studies suggest that an intricate regulatory network coupling extrinsic signaling pathways and intrinsic transcriptional regulators governs OL production.

Here, we tested the role of PRC2 in neuro-glial fate switches via cell-type and temporal-specific inactivation of PRC2 in mice. We show that PRC2 is required for the developmental progression from OPCs to myelinating OLs, but not for OPC generation or for motor neuron differentiation. We further demonstrate the molecular mechanism underlying this specific action of PRC2. PRC2 deletion resulted in a loss of OLs and severe dysmyelination, concomitant with the induction of Notch and Wnt pathways and astrocytic genes. Our genome-wide analyses suggest that during OL differentiation, PRC2 is recruited to and represses Notch and Wnt signaling genes. Moreover, our data revealed that in the PRC2-deficient OL lineage, aberrantly enhanced Notch and Wnt pathways contribute to OL differentiation deficits, whereas Notch signaling, but not Wnt signaling, is the main driver of ectopic astrocytic differentiation. Thus, PRC2-directed downregulation of the Notch pathway is critical for the timely activation of the molecular programs for myelin gene expression and the inhibition of erroneous astroglial fate switch. Altogether, our results uncover striking specificity in the requirement of PRC2 in glial cell fate choices and provide

Author Manuscript Author Manuscript Author Manuscript Author Manuscript

critical insights into epigenetic regulatory mechanisms that determine the timing of stepwise differentiation of neural cell types.

RESULTS

Ezh2 Is Vital for the Timely Generation of OLs, but Not of OPCs

During spinal cord development, the progenitor cells in the pMN and p3 domains give rise to motor neurons and V3 interneurons, respectively (Lee and Pfaff, 2001). Once the neurogenic phase ends, the progenitor cells in the pMN and p3 domains produce OLs and astrocytes, respectively (Hochstim et al., 2008; Lee and Pfaff, 2001; Lu et al., 2002; Takebayashi et al., 2002; Zhou and Anderson, 2002). To test whether PRC2 plays a role during dynamic neuro-glial fate switches that produce neurons, OLs, and astrocytes, we examined the expression pattern of Ezh2, the predominant H3K27 methyltransferase enzyme in PRC2, in the developing chick spinal cord. Ezh2 is highly expressed in neural progenitors in the ventricular zone but is downregulated as progenitors migrate laterally and differentiate into neurons (Figure 1A). However, Ezh2 expression is maintained in OL lineage cells, including migratory OPCs and myelin basic protein (Mbp)$^+$ OLs (Figure 1). Similarly, Ezh2 is highly expressed in Olig2-expressing OL lineage cells in the white matter of the developing mouse spinal cord (Figure S1), suggesting a possible role of Ezh2 in the OL lineage.

Next, we deleted Ezh2 from neural progenitors in the pMN and p3 domains using the Olig2-Cre driver (Dessaud et al., 2007; Shen et al., 2008). In *Ezh2$^{f/f}$;Olig2-Cre* conditional knockout (*Ezh2-cKO$^{\Delta Olig2}$*) mice, the H3K27me3 mark drastically decreased in the pMN and p3 domains and motor neurons at embryonic day (E) 12.5 (Figure 2A). These data indicate that Ezh2 is a predominant H3K27 methyltransferase in the embryonic spinal cord and it was inactivated in pMN and p3 cells before or during motor neuron production in *Ezh2-cKO$^{\Delta Olig2}$* mice. However, despite the marked reduction of H3K27me3 marks in motor neurons, we did not detect a substantial change in the generation of Olig2$^+$ pMN progenitors or motor neuron subtypes in *Ezh2-cKO$^{\Delta Olig2}$* mice (Figure S2).

The H3K27me3 mark remained absent from the OPCs and OLs in E18.5 *Ezh2-cKO$^{\Delta Olig2}$* mice (Figure 2A), indicating that Ezh2 is a critical enzyme for generating the repressive H3K27me3 mark in the OL lineage in embryos. Next, we monitored the property of OPCs and OLs using the OPC marker platelet-derived growth factor receptor α (PDGFRα) and the OL markers Mbp and proteolipid protein (Plp) 1. PDGFRα$^+$ OPCs exhibited no significant change in *Ezh2-cKO$^{\Delta Olig2}$* mice (Figures 2B and 2C), suggesting that the elimination of Ezh2 from pMN cells does not interfere with OPC fate specification. In contrast, Mbp$^+$/Plp1$^+$ OLs were markedly reduced at E18.5 and remained decreased at postnatal day (P) 3 in *Ezh2-cKO$^{\Delta Olig2}$* mice (Figures 2B and 2C). By P10, however, OL generation was restored in *Ezh2-cKO$^{\Delta Olig2}$*, comparable to control littermates (Figure 2B). These results indicate that the generation of OLs, not OPCs, is delayed in the absence of Ezh2.

The postponed OL generation in *Ezh2-cKO$^{\Delta Olig2}$* mice prompted us to ask whether Ezh2 in OPCs is required for the timely differentiation of OPCs or whether Ezh2 action is needed in neural progenitor cells before their differentiation to OPCs. To distinguish between these possibilities, we deleted *Ezh2* using OL-lineage-specific *Olig1-Cre* that becomes active in

Author Manuscript Author Manuscript Author Manuscript Author Manuscript

OPCs (Xin et al., 2005). As predicted, the H3K27me3 mark was abolished from OPCs and OLs, but not from neural progenitors and motor neurons, in *Ezh2$^{f/f}$;Olig1-Cre* (*Ezh2-cKO$^{\Delta Olig1}$*) (Figure S3A). Despite the difference in the timing of Ezh2 inactivation, the phenotypes of *Ezh2-cKO$^{\Delta Olig1}$* and *Ezh2-cKO$^{\Delta Olig2}$* mice were remarkably similar. In *Ezh2-cKO$^{\Delta Olig1}$* mice, OL differentiation was substantially compromised without a significant change in OPCs at E18.5 and P3, and then OLs were recovered by P10 (Figures S3B and S3C). These results indicate that the differentiation and maturation of OLs were delayed in both *Ezh2-cKO$^{-\Delta}$Olig2* and *Ezh2-cKO$^{\Delta Olig1}$* mice and that these deficits were eventually remedied by P10. Altogether, our data establish that Ezh2, catalyzing the H3K27me3 mark, plays a crucial role in promoting the timely progression of OPCs to myelinating OLs in a specific developmental window, but it is dispensable for the generation of OPCs.

PRC2 Is Required for the Generation of OLs and Myelination

The clearly delayed but restored OL formation in *Ezh2-cKO$^{\Delta Olig1}$* and *Ezh2-cKO$^{\Delta Olig2}$* mice prompted us to ask whether other chromatin regulators counterbalance the loss of Ezh2 at a perinatal stage. H3K27me3 levels begun to rise in Olig2$^+$ OL lineage cells at P3 in *Ezh2-cKO$^{\Delta Olig2}$* mice, although overall H3K27me3 levels in Olig2$^+$ cells of *Ezh2-cKO$^{\Delta Olig2}$* mice remained reduced compared with control mice (Figures 2A and 3B), suggesting that Ezh1, the only other H3K27 methyltransferase, may compensate for Ezh2 deficiency by P3 and contribute to the recovery of postnatal OL differentiation in Ezh2-deficient mice. Supporting this possibility, Ezh1 was upregulated in the OL lineage cells in the white matter at P3, whereas its expression was below detection level in the white matter of the spinal cord at E18.5 (Figure S4).

Our data raised the possibility that both PRC2-Ezh1 and PRC2-Ezh2 are involved in the formation of myelinating OLs. To inactivate both PRC2s, we deleted *Eed*, a common component of PRC2-Ezh1 and PRC2-Ezh2 (Margueron and Reinberg, 2011), using *Olig2-Cre*. In *Eed$^{f/f}$;Olig2-Cre* (*Eed-cKO$^{\Delta Olig2}$*) mice, the H3K27me3 mark was eliminated from neural progenitors in pMN and p3 domains and markedly reduced in motor neurons at E12.5 (Figure 3A). The H3K27me3 mark remained extremely low in the OL lineage even in P3 *Eed-cKO$^{\Delta Olig2}$* mice (Figures 3A and 3B), unlike *Ezh2-cKO$^{\Delta Olig2}$* mice that show partially restored levels of H3K27me3 at P3 (Figures 2A and 3B), supporting the possibility that PRC2-Ezh1 triggers H3K27 methylation in Ezh2 null OL lineage cells at P3.

Eed-cKO$^{\Delta Olig2}$ mice did not show changes in the generation of Olig2$^+$ pMN progenitors, Hb9$^+$ motor neurons, or motor neuron subtypes (Figure S5). PDGFRα$^+$ OPCs were also produced and migrated normally in *Eed-cKO$^{\Delta Olig2}$* mice (Figure 3B; Figure S6A), suggesting that PRC2 is dispensable for the production and migration of OPCs. There were no significant changes in proliferation and cell death of OPCs (Figures S6B–S6D). However, Mbp$^+$/Plp1$^+$ OLs were markedly reduced at P3 and did not recover even at P10 in the spinal cord of *Eed-cKO$^{\Delta Olig2}$* mice (Figure 3B). Consistently, unlike the optic nerves of control mice that were opaque, the optic nerves of *Eed-cKO$^{\Delta Olig2}$* mice were transparent, indicating a lack of myelination (Figure S6E). Furthermore, electron microscopy (EM) analyses revealed a severe deficiency of axonal myelination in the spinal cord and optic nerve of *Eed-cKO$^{\Delta Olig2}$* mice (Figure 3D). *Eed-cKO$^{\Delta Olig2}$* mice began to show typical dysmyelination

Author Manuscript Author Manuscript Author Manuscript Author Manuscript

phenotypes, including ataxia, tremors, and seizures, at P10 and died between P13 and P17 (Video S1). These data establish that PRC2 is required for the formation of OLs, but not for the generation of OPCs, and that PRC2-Ezh1 and PRC2-Ezh2 act redundantly to promote postnatal myelination within the CNS in mice.

PRC2 Is Essential to Trigger the Molecular Program for OL Differentiation and Myelination

To understand the mechanistic basis underlying dysmyelination phenotypes of *Eed-cKO$^{\Delta Olig2}$* mice, we immunopanned O4^{+}/GalC^{-} OPCs from *Eed-cKO$^{\Delta Olig2}$* and control brains and induced their synchronous differentiation into OLs (Dugas and Emery, 2013). Under the proliferation condition, both Eed-deficient and control OPCs remained positive for Olig2, NG2, and Ki67 (Figures 4A and 4B), indicating that PRC2 is not needed for the proliferation of OPCs. Despite comparable proliferation, the number of Eed-deficient OPCs increased more slowly than the number of control OPCs. The live-dead assay revealed increased cell death in *Eed-cKO$^{\Delta Olig2}$* cells under the proliferation condition (Figure S7A), suggesting that PRC2 plays a role in the survival of OPCs *in vitro*. Upon initiation of OL differentiation by withdrawing PDGF, both control and *Eed-cKO$^{\Delta Olig2}$* cells expressed Cnp, a marker of immature OLs (iOLs), by 2 differentiation days *in vitro* (DD) (Figures 4C and 4D). However, relative to control cells, *Eed-cKO$^{\Delta Olig2}$* cells exhibited a substantial reduction in Cnp and Mbp expression levels and extension and networks of cellular membrane sheets (Figures 4C and 4D), suggesting that Eed-deficient OPCs failed to differentiate into mature OLs or fully execute the myelination program. These data highlight a critical role of PRC2 in triggering OL differentiation.

To determine the downstream target genes and signaling pathways of PRC2 that mediate OL development, we deduced PRC2-dependent transcriptome changes in acutely isolated OPCs and iOLs at 2 DD using RNA sequencing (RNA-seq) analyses. 96% and 88% of differentially expressed genes (absolute log2 fold change ≥ 1 and false discovery rate [FDR] ≤ 0.05) were upregulated in Eed-deficient OPCs and iOLs, respectively, compared with control (*Eed$^{fl/+}$;Olig2-Cre*) OPCs and iOLs (Figures 4E and 4F; Tables S1 and S2), consistent with the notion that PRC2 primarily acts as a repressor (Margueron and Reinberg, 2011). The expression of two OPC marker genes, PDGFRα and NG2 (Cspg4), showed no significant change in Eed-deficient OPCs and a mild increase in Eed-deficient iOLs, consistent with defects in transitions of OPCs to OL states in *Eed-cKO$^{\Delta Olig2}$* mice (Figure 4G). The myelin genes, such as Mbp, Plp1, Mag, Mog, and Mobp, were markedly downregulated in Eed null iOLs (Figure 4G). Notably, Eed null iOLs failed to induce many transcription factor genes critical for OL development, such as Myrf, Zfp488, Tcf7l2, Nkx2–2, and Sox10 (Figure 4G), suggesting that PRC2 is crucial to trigger the transcription program driving OL differentiation in OPCs upon arrival of differentiation signals.

Altogether, our data support the notion that PRC2 is required for prompting the molecular program for OL terminal differentiation and myelination in the OL lineage.

Astrocyte Gene Program Was Aberrantly Induced in the Eed-Deficient OL Lineage

Interestingly, RNA-seq analyses revealed that the astrocytic genes Gfap and Mfge8 (Chaboub et al., 2016) were significantly upregulated in *Eed-cKO$^{\Delta Olig2}$* iOLs compared with

Author Manuscript Author Manuscript Author Manuscript Author Manuscript

control iOLs (Figure 4G; Table S2). Furthermore, the astrocytic-fate-promoting transcription factor NFIA, which operates downstream of Notch (Deneen et al., 2006; Kang et al., 2012; Namihira et al., 2009), was substantially increased in Eed-deficient iOLs (Figure 4G), suggesting that the astrocyte differentiation program was aberrantly induced in PRC2-deficient OL lineage cells.

Consistent with astroglial gene induction, $Olig2^{+}GFAP^{+}$ cells increased in Eed null iOLs, relative to control iOLs, under the differentiation condition (Figures 5A and 5B). Likewise, a significant increase of $Olig2^{+}GFAP^{+}$ cells was observed in P3 *Eed-cKO*$^{\Delta Olig2}$ spinal cord (Figures 5C and 5D). Altogether, our data indicate that at least a subset of PRC2-deficient OL lineage cells trigger the astrocyte differentiation pathway.

PRC2 Suppresses Notch and Wnt Signaling Pathways

Developmental signaling cues play important roles in modulating the progression of OL fate specification and differentiation (He and Lu, 2013). Combined with the notion that PRC2 predominantly acts as a transcriptional repressive complex (Margueron and Reinberg, 2011), our data raised the possibility that PRC2 inhibits developmental signals that suppress OL differentiation and/or promote astroglial differentiation in OL lineage cells. To determine which signaling pathways are augmented in Eed-deficient OL lineage cells, we performed Gene Ontology (GO) analyses on the upregulated genes in *Eed-cKO*$^{\Delta Olig2}$ cells. The genes implicated in Notch, Wnt, and BMP signaling pathways were significantly upregulated in *Eed-cKO*$^{\Delta Olig2}$ OPCs, and this trend was reinforced in Eed null iOLs (Figures 6A and 6B; Table S3), suggesting that Notch, Wnt, and BMP signals are enhanced in PRC-deficient OL lineage cells.

Enhanced Notch, Wnt, and BMP signaling pathways have been shown to prevent OL differentiation while being implicated in astrocytic differentiation (Fancy et al., 2009; Genoud et al., 2002; Gomes et al., 2003; He and Lu, 2013; Nakashima et al., 1999; Namihira et al., 2009; Samanta and Kessler, 2004; Wang et al., 1998; Ye et al., 2009). Thus, we tested whether these developmental signals are aberrantly activated in the PRC2-deficient OL lineage using immunostaining analyses with antibodies against active Notch1, active β-catenin, and phosphorylated Smad1/5/8. We also assessed the activity of the Janus kinase (Jak)-Stat pathway, which induces astrocytic differentiation of neural progenitors (He et al., 2005; Nakashima et al., 1999), using the antibody against phosphorylated Stat3. Notch and Wnt pathways were clearly augmented in Eed null iOLs, whereas neither the phosphorylated Smad1/5/8 nor the phosphorylated Stat3 signal was substantially elevated (Figures 6C and 6D; Figure S7B). In addition, NFIA, downstream of Notch (Namihira et al., 2009), was upregulated in Eed null iOLs (Figures 6C and 6D). Our data indicate that PRC2 plays a role in suppressing Notch and Wnt signaling pathways in the OL lineage.

The RNA-seq analyses revealed Notch signal transduction genes, including Notch receptors, Notch ligands, and Notch downstream effectors, were upregulated in Eed-deficient OL lineage cells (Figure 6E). Likewise, Wnt signal transduction genes, such as Fzd and Rspo receptors, Lef1 transcription factor, Wnt ligands, and Wnt downstream effector genes Id1, Id2, and Id4, were induced in Eed null OL lineage cells (Figure 6E). To test whether PRC2 controls the expression of Notch and Wnt pathway genes by directly binding to the genes,

Author Manuscript Author Manuscript Author Manuscript Author Manuscript

we performed chromatin immunoprecipitation sequencing (ChIP-seq) analyses with antibodies against Suz12 and Eed, the two critical common components of Ezh2- and Ezh1-containing PRC2s (Margueron and Reinberg, 2011), in P3 spinal cords. The genome-wide binding patterns of Suz12 and Eed were highly similar (Figure 6F; Figure S8), confirming that they act together as components of PRC2. Most upregulated genes in Eed null OPCs or iOLs were annotated to Suz12-bound ChIP-seq peaks, whereas most downregulated genes in Eed null OL lineage cells were not associated with Suz12-bound ChIP-seq peaks (Figures 6G and 6H; Table S4). These data suggest that PRC2 represses many genes, which were de-repressed in Eed null OPCs and OLs via direct binding of Suz12 and Eed, alone or together, and bound most Notch and Wnt pathway genes that were upregulated in Eed-deficient iOLs (Figure 6F; Figures S8A and S8B). To test PRC2 binding to these genes in the OL lineage, we performed ChIP with Suz12 antibody in OPCs and iOLs and found that Suz12 occupied the select Notch and Wnt genes in OL lineage cells (Figure 6I).

Next, to test whether PRC2-mediated repression of Notch and Wnt pathway genes involves the H3K27me3 decoration, we reanalyzed the published the H3K27me3 ChIP-seq dataset in rat OPCs (Liu et al., 2015) and found that most PRC2-target Notch and Wnt pathway genes are marked by H3K27me3 in the OL lineage (Figures S8A and S8C). Altogether, these data demonstrate that PRC2 suppresses Notch and Wnt signaling activities during differentiation of OPCs to OLs, at least partly, by directly binding and suppressing Notch and Wnt pathway genes.

The Notch-NFIA Axis Is Aberrantly Activated in *Ezh2*-and *Eed*-Deficient OL Lineage Cells

The Notch signaling pathway has been shown to promote the astrocytic fate by elevating NFIA expression (Namihira et al., 2009). The elevated levels of both Notch signaling and NFIA in PRC2 null OLs differentiated *in vitro* led us to hypothesize that the Notch-NFIA axis is de-repressed in OL-lineage-committed cells when PRC2 is eliminated, thus contributing to severe dysmyelination phenotypes of PRC2-deficient mice. To test this hypothesis, we investigated whether the NFIA expression is upregulated in the OL lineage cells in *Ezh2-cKO*$^{\Delta Olig2}$ and *Eed-cKO*$^{\Delta Olig2}$ mice and whether the deviant induction timing and level of NFIA predict the disparity of severity in OL phenotypes between these mouse models. In the developing spinal cord, ~30% of Olig2^{+} OL lineage cells express low-level NFIA at E18.5 and P3 (Figure 7A), consistent with reports that NFIA is vital for establishing glial progenitors and it is repressed as OPCs differentiate to OLs in the glial lineage (Deneen et al., 2006; Fancy et al., 2012). In *Ezh2-cKO*$^{\Delta Olig2}$, both the fraction of NFIA-expressing Olig2^{+} OL lineage cells and the level of NFIA expression in these cells increased at E18.5 relative to control mice but reduced to the control level by P3 (Figures 7A and 7C). These data indicate that in the absence of Ezh2, the *NFIA* gene was transiently upregulated in OL lineage cells but repressed by P3, when Ezh1 is induced in the OL lineage, preceding the recovery of myelination. In contrast, in *Eed-cKO*$^{\Delta Olig2}$ mice, NFIA expression is continuously and substantially elevated at P3 (Figures 7B and 7C) before severe dysmyelination phenotypes emerge. Altogether, our data suggest that the Notch-NFIA axis is aberrantly activated in PRC-defective OL lineage cells in a manner highly correlated to the myelination defects. Our data further suggest that PRC2 plays a critical role for the timely repression of the Notch-NFIA axis in OPCs and continuous inhibition of this axis in

Author Manuscript Author Manuscript Author Manuscript Author Manuscript

OL lineage cells postnatally. It is also notable that in Ezh2-deficient OL lineage cells, the restoration of NFIA suppression precedes a rescue of Mbp^+ OL differentiation at P10, suggesting that the delay in Notch-NFIA suppression contributes to suspended production of OLs in *Ezh2-cKO$^{\Delta Olig2}$* mice.

To test whether the prolonged expression of NFIA prevents the differentiation of OPCs to myelinating OLs in PRC2 null mice, we monitored the effect of enforced NFIA expression on endogenous OL differentiation in the developing spinal cord using *in ovo* electroporation. Maintained expression of NFIA resulted in a striking reduction of Mbp^+ OLs but did not decrease the number of $PDGFR\alpha^+$ OPCs (Figure S9A), suggesting that downregulation of the Notch-NFIA axis is a critical step to allow the transition of OPCs to OLs, but not the production of OPCs.

Olig2 is capable of triggering both OPC generation and OPC differentiation to OLs (Lu et al., 2002; Zhou and Anderson, 2002). Given the increased NFIA levels in $Olig2^+$ OL lineage cells in PRC2 null mice, we tested whether NFIA impairs the ability of Olig2 to induce ectopic OPCs or OLs using *in ovo* electroporation. When co-expressed with NFIA, Olig2 failed to induce Mbp^+ OLs, but it was still capable of inducing $PDGFR\alpha^+$ OPCs (Figures S9B and S9C), indicating that the increased level of NFIA in $Olig2^+$ OL lineage cells is capable of blocking terminal OL differentiation and myelination but does not inhibit OPC fate.

The Notch Is a Primary Repressive Target of PRC2 in Promoting OL Differentiation and Blocking the Astrocytic Fate

Our results led us to test whether the repression of aberrantly enhanced Notch or Wnt signaling can restore impaired OL differentiation in PRC2-deficient OPCs. To this end, we isolated Eed-deficient and control OPCs and subjected them to OL differentiation in the presence of the Notch inhibitor LY411575 alone, the Wnt inhibitor XAV939 alone, the combination of both inhibitors, or vehicle. We then monitored their differentiation status at 3 DD. Interestingly, both Notch inhibition and Wnt inhibition significantly rescued Mbp expression and OL morphology in the Eed null OL lineage, and simultaneous suppression of Notch and Wnt further enhanced OL differentiation (Figures 7D and 7E), suggesting the increase of Notch and Wnt signaling upon a loss of PRC2 contributes to the halted OL differentiation of Eed null cells. Notch inhibitor, but not Wnt inhibitor, blocked aberrant induction of the $GFAP^+$ astrocyte differentiation program (Figures 7D and 7F), suggesting that Notch is a main pathway driving erroneous astrocytic differentiation. These data establish that the Notch pathway is a primary repressive target of PRC2 in promoting OL differentiation and suppressing the astrocytic fate and that PRC2-directed repression of the Wnt pathway is vital for timely OL differentiation.

DISCUSSION

The myelination of CNS requires highly orchestrated stepwise processes by which neural progenitors differentiate into proliferating OPCs and subsequently into myelinating OLs. These dynamic processes accompany profound global changes in chromatin architecture and gene expression. Here we report a novel action of PRC2, the H3K27 methyltransferase

Author Manuscript Author Manuscript Author Manuscript Author Manuscript

complex, as an epigenetic gatekeeper in the OL lineage and the underlying molecular mechanism. PRC2 controls the timing of OL production from OPCs, but not the timing of OPC generation from neural progenitors, although it is continuously expressed and generates H3K27me3 marking from the neural progenitor stage to the OL stage. The specific requirement for PRC2 at the onset of OL formation from OPCs suggests that PRC2 plays a specific action in each cell lineage, rather than acting as a general silencer of developmental genes. We found that PRC2 promotes the OL differentiation and myelination program by suppressing Notch and Wnt signaling pathways. Our study further revealed that PRC2 prevents OPCs from erroneously adopting an astroglial fate by suppressing the Notch-NFIA axis, thus reinforcing the OL lineage commitment. Therefore, PRC2 serves as a critical component of the intricate regulatory network for OL fate decision and maturation, which couples intrinsic transcriptional regulators and extrinsic signaling pathways.

The eukaryotic chromatin structure provides a sophisticated layer of gene regulation. For the past two decades, histone modification has emerged as a primary mechanism to control chromatin structure and gene expression (Kouzarides, 2007). In particular, H3K27me3 marks repressive and poised chromatin. H3K27me3 is absent from lower eukaryotic model organisms, such as *Schizosaccharomyces cerevisiae* and *Schizosaccharomyces pombe*, whereas it was found in various animals and plants (Lachner et al., 2004), suggesting that H3K27me3 may play a major role in the development of multicellular organisms. PRC2 possesses H3K27 methyltransferase activity and mainly acts as a transcriptional repression complex that is important to maintain a cellular identity (Margueron and Reinberg, 2011). Past studies have revealed a range of actions of PRC2 in diverse cellular contexts, including cell-cycle control, genomic imprinting, stem cell plasticity, and cancer (Margueron and Reinberg, 2011). In embryonic stem cells, PRC2 is important to repress developmental genes and maintain cell pluripotency (Boyer et al., 2006; Lee et al., 2006; Pietersen and van Lohuizen, 2008). When neural progenitor cells are cultured *in vitro*, Ezh2 is highly expressed in progenitors but is downregulated in neurons and astrocytes (Sher et al., 2008). The downregulation of Ezh2 was necessary for the production of astrocytes in cultured neural progenitor cells (Sher et al., 2008), which is consistent with our finding that PRC2 represses the astrocytic-fate-driving Notch-NFIA axis. In contrast to neurons and astrocytes, Ezh2 expression is maintained as neural progenitor cells differentiate into OPCs and OLs, both *in vivo* (Figure 1; Figure S1) and in cultured cells (Sher et al., 2008), but the *in vivo* role of PRC2 in the OL lineage remained ambiguous, partly because a report of strong myelination phenotypes in PRC2-deficient animal models has been lacking. By systematically analyzing multiple mouse lines that inactivate only PRC2-Ezh2 or both PRC2-Ezh2 and PRC2-Ezh1, we addressed this critical question. Our analyses of *Ezh2*-cKO mice with *Olig1-Cre* or *Olig2-Cre* revealed that OL differentiation was delayed but eventually remedied in *Ezh2*-cKO mice, allowing the mice to live into adulthood. In contrast, the inactivation of both PRC2-Ezh2 and PRC2-Ezh1 resulted in severe dysmyelination and death in mice. Our data indicate that Ezh2 is the main enzyme to deposit the H3K27me3 mark in the OL lineage during embryonic development, but both Ezh1 and Ezh2 are capable of maintaining the overall level of H3K27me3 in OPCs and OLs after birth. Our study also suggests that *de novo* synthesis of the H3K27me3 mark by PRC2 is crucial to set the schedule of differentiation for specific, but not all, cell types, supporting

Author Manuscript Author Manuscript Author Manuscript Author Manuscript

the idea that H3K27me3 is subject to highly dynamic regulation during differentiation and development, rather than serving as a stable marker for the repressive chromatin domain. PRC2 activity is dispensable for the generation of OPCs emerging from neural progenitors in the ventricular zone, whereas it is required for differentiation and maturation of OLs. In light of this, it is noteworthy that H3K27me3 levels substantially increase as OPCs differentiate into myelinating OLs (He et al., 2017; Liu et al., 2015).

How does PRC2 promote the timely transition of OPCs to OLs and suppress astroglial fate? Our results indicate that the Notch and Wnt pathways are major repressive targets of PRC2 during OPC differentiation to OLs. Notch signaling activation in neural progenitors instructs the commitment of glial fate and promotes OPC specification while inhibiting neuronal differentiation (Kim et al., 2008; Park et al., 2005). However, the continuous activation of Notch signaling or its effector Hes5 in OPCs interferes with OL differentiation (Kondo and Raff, 2000a; Liu et al., 2006; Wang et al., 1998). Consistent with the notion that NFIA acts downstream of Notch (Namihira et al., 2009), overall NFIA action resembles the Notch activation in OPCs, in which NFIA preserves the OPC state and represses premature OPC differentiation to OLs by suppressing myelin genes and antagonizing Sox10 activity (Fancy et al., 2012; Glasgow et al., 2014). We and others found that sustained expression of NFIA blocks OL differentiation and myelination in both development (Figure S9) and remyelination conditions (Fancy et al., 2012). High-level Notch activity or NFIA promotes migration and differentiation of astrocytes at the expense of OL fate (Kang et al., 2012; Namihira et al., 2009). Altogether, to enable the differentiation of OPCs to OLs while inhibiting unwanted upregulation of astrocytic genes, it is crucial to suppress the Notch-NFIA axis. Several reports also show that the Wnt-β-catenin-Lef1 signaling cascade inhibits OPC differentiation and myelination (Fancy et al., 2009; Shimizu et al., 2005; Ye et al., 2009). Our data suggest that PRC2 plays an essential role in repressing the Notch-NFIA and Wnt pathways to drive the transition of OPCs to the myelinating OL state and to prevent astroglial fate switch. Aberrant activation of Notch or Wnt signals was found in the hypomyelination diseases (Fancy et al., 2009; Lock et al., 2002; Petersen et al., 2017), suggesting the deleterious effects of elevated Notch and Wnt signals on myelination. Thus, boosting PRC2 activity to repress Notch-NFIA and Wnt may represent a novel therapeutic venue to facilitate remyelination in adults.

Our study suggests that PRC2 binds and represses a subset of Notch and Wnt signaling genes in OLs. This raises the question of how PRC2 is recruited to a specific set of target genes during OL differentiation. A recent study of OL-lineage-enriched long noncoding RNAs (lncRNAs) (He et al., 2017) points to the possibility that lncRNAs whose expression is induced during the OPC-to-OL transition play roles in targeting PRC2 to the OPC maintenance genes. As *lncOL1*, the OL-enriched lncRNA, interacts with Suz12 (He et al., 2017), *lncOL1* may mediate the recruitment of PRC2 to some Notch or Wnt genes. Notably, *lncOL1*-deficient mice displayed a delay in OL differentiation and myelination, but their myelination was fully recovered by adulthood (He et al., 2017). Given that the severity of the inactivation of PRC2 in the OL lineage is far greater than the removal of *lncOL1*, it is likely that PRC2 also employs lncRNA-independent mechanisms or multiple lncRNAs in directing OL differentiation and myelination programs.

Author Manuscript Author Manuscript Author Manuscript Author Manuscript

STAR★METHODS

RESOURCE AVAILABILITY

Lead Contact—Further information and requests for resources and reagents should be directed to and will be fulfilled by the Lead Contact Soo-Kyung Lee (slee229@buffalo.edu). There are no restrictions on any data or materials presented in this paper.

Materials Availability—This study did not generate new unique reagents.

Data and Code Availability—The accession number for the RNA-seq and ChIP-seq datasets reported in this paper is GEO: GSE130628.

EXPERIMENTAL MODEL AND SUBJECT DETAILS

Mouse lines—*Ezh2*$^{flox/flox}$, *Eed*$^{flox/flox}$, *Olig2-Cre*, and *Olig1-Cre* mouse lines were described previously (Dessaud et al., 2007; Shen et al., 2008; Xin et al., 2005; Yu et al., 2009). Animals were housed and analyzed according to the Institutional Animal Care and Use Committee (IA-CUC) guidelines. For timed mating, embryos were considered to be at 0.5 day of gestation (E0.5) on the day when a vaginal plug was detected.

METHOD DETAILS

Immunohistochemistry and *in situ* hybridization (ISH)—The chicken and mouse tissues were collected at various stages, fixed in 4% paraformaldehyde, immersed in 30% sucrose, and embedded in OCT for cryosectioning and subsequent analyses. Assays were performed as described (Clovis et al., 2016). Briefly, for immunohistochemistry, 12 μm cryosectioned slices were incubated with the primary antibodies overnight at 4°C using 10% FBS blocking buffer (10% Fish gelatin, 0.3% Triton X-100 in PBS buffer). Then Fluorophore-conjugated species-specific secondary antibodies were used as recommended (Jackson ImmunoResearch laboratories). Zeiss Imager Z2 fluorescence microscope with Apotome and Nikon Eclipse Ti confocal microscope were used for imaging. Primary antibodies for immunostaining are listed in the Key Resources Table.

For *in situ* hybridization analysis, embryos were harvested as above, and cryosectioned at 18 μm. As described, transverse sections were post-fixed, permeabilized with proteinase K treatment, acetylation treated and then hybridized overnight with digoxigenin-labeled riboprobes at 68°C. After washed with 0.2X SSC buffer at 65°C for 2 hours and then blocked with 4% BSA in TBS buffer (0.1M Tris, 0.15M NaCl, pH7.5), sections were incubated with anti-digoxigenin alkaline phosphatase-conjugated antibody (Roche) in 2% BSA TBS. Color reaction was developed with NCIP/NBT substrates (Roche). The plasmids to make Digoxigenin-labeled probes complementary to mouse or chick PDGFRα, MBP, PLP were kindly provided by Dr. Benjamin Deneen. Mouse Ezh2 fragment (1–867bp) and Ezh1 fragment (1–867bp) were cloned into pBluescript vector to generate ISH probes.

Electron microscopy—Tissue preparation and electron microscopy (EM) were performed as previously described with minor modification (Aicher et al., 2012; Yu et al., 2013). Mice were anesthetized and then perfused briefly with 0.1 M phosphate buffer (PB,

Author Manuscript Author Manuscript Author Manuscript Author Manuscript

pH 7.4), followed by 2% paraformaldehyde (PFA) and 2% glutaraldehyde in 0.1 M PB for 10 min. Spinal cords and optic nerves were dissected and then post-fixed in fresh 2% PFA for 30 min at room temperature. Thoracic regions of spinal cords were sectioned on a vibrating microtome at 40 microns. Spinal cord sections and whole optic nerves were rinsed briefly in 0.1 M PB and then incubated in 1% osmium tetroxide in 0.1 M PB for 30 min. After osmication, tissues were rinsed again in 0.1 M PB and dehydrated at 5 minutes each through a graded series of ethanol. Tissues were placed in fresh propylene oxide (PO) twice for 10 min then incubated overnight in a 1:1 mixture of PO and EMBed 812 (Electron Microscopy Sciences, Hatfield, PA). Tissues were placed in fresh EMBed 812 resin for 2 hours then spinal cord sections were flat embedded between two sheets of Aclar plastic and optic nerves were embedded in plastic molds. Embedded tissue was placed in a 60°C oven for 48 hours. Spinal cord sections were glued to plastic blocks formed in Beem capsules and trimmed to include the ventral spinal cord as the region of interest. Optic nerves were trimmed to provide crosssections of the tissue. Optic nerves and spinal cords were sectioned on an ultramicrotome (Leica UC6, Leica Microsystems Inc., Buffalo Grove, IL) at 200 nm for toluidine blue staining and at 60 nm for EM. Sections for EM were collected onto copper grids and counterstained with uranyl acetate and Reynolds lead citrate. Images were taken on an FEI Tecnai 12 electron microscope.

Oligodendrocyte precursor cell (OPC) isolation and *in vitro* differentiation— Mouse OPCs were isolated as described (Dugas and Emery, 2013). Briefly, mouse brains at P6–7 were diced into about $1mm^3$ chunks and then enzymatically digested in the papain solution at 34°C for 90 min under 5% CO_2/95% O_2. The digested and triturated cell suspension was subsequently immunopanned by anti-Ran-2 (ATCC® TIB-119) and anti-GalC (Millipore MAB342) antibodies in the panning buffer to remove astrocytes and oligodendrocytes, followed by positive selection with anti-O4 antibody (Millipore MAB345). The final O4+ OPC cells were harvested in TRIzol for RNA extraction or trypsinized for plating. For OPC culture, cells were seeded at a density of 10,000 cells in the 24-well plates coated with Poly-D-Lysine (PDL, 10μg/ml) and cultured in DMEM-Sato base growth medium supplemented with neurotropin-3 (NT-3, 1ng/ml, PeproTech), Forskolin (4.2μg/ml, Sigma), CNTF (10ng/ml, PeproTech) and PDGF-AA (10 ng/ml, PeproTech). OPCs were harvested for immunostaining after 2 days of proliferation. For OPC differentiation, cells were seeded at a density of 50,000 cells in the 24-well plates coated with PDL in the differentiation medium ((DMEM-Sato base growth medium supplemented with NT-3, Forskolin, CNTF and triiodothyronine (T3, 40ng/ml, Sigma) instead of PDGF-AA)). Acutely isolated OPCs started to differentiate upon addition of differentiation medium in the 24-well plates and cells were harvested for RNA-seq or immunostaining after two or three days of differentiation, as indicated in the figure or text. For the experiments with Notch and Wnt inhibitors, we isolated OPCs from four *Eed-cKO*$^{\Delta Olig2}$ and three control mice, and cultured them in the differentiation medium, which contains DMSO vehicle (DMS/o), 0.2μM of Notch inhibitor LY411575, 0.5μM of Wnt inhibitor XAV939, or both inhibitors, for three days. Under this condition, neither Notch inhibitor nor Wnt inhibitor caused cell death during OPC differentiation.

Author Manuscript Author Manuscript Author Manuscript Author Manuscript

RNA-seq analysis—For OPC RNA-seq samples, OPCs were isolated from three *Eed-cKO$^{\Delta Olig2}$* and two control (*Eed$^{f/f}$;Olig2-Cre*) mice using the immunopanning method described above. Then, the five samples were subject to RNA extraction without an *in vitro* culture step. For OL RNA-seq samples, OPCs were isolated from two *Eed-cKO$^{\Delta Olig2}$* and two control (*Eed$^{f/f}$;Olig2-Cre*) mice using the immunopanning method and differentiated to OLs *in vitro* for two days. Then, the four OL samples were subject to RNA extraction. The cells were harvested in TRIzol reagent (Thermofisher), and total RNA was extracted following the instruction manual. For RNA > 100ng, the libraries were prepared using RNA-seq Stranded Library kit (Illumina TruSeq with PolyA selection). For RNA < 100ng, Clontech SMARTer RNA kit was used to construct RNA-seq Library.

Sequencing adapters that existed in the raw reads were trimmed by cutadapt ver 1.14 (Martin, 2011). The trimming option was used for the common adaptor sequence of the Illumina TruSeq adapters. High quality reads were obtained through trimming and then mapped to the reference genome by STAR ver 2.6.0 (Dobin et al., 2013). The quality of alignment was checked by QualiMap ver 2.2.1 (García-Alcalde et al., 2012). To quantify the mapped reads on the reference genome into the gene counts, featureCounts (Liao et al., 2014) in subread ver 1.6.2 with the strand-specific library option to reverse strand was used. Gene annotation were performed in the gtf format of the NCBI (https://www.ncbi.nlm.nih.gov/) mm10 reference genome.

The Differentially Expressed Genes (DEG) between *Eed-cKO$^{\Delta Olig2}$* and control samples were analyzed using edgeR (Robinson et al., 2010) that are R package in bioconductor. Genes with zero and low expression value were filtered and then normalization process was performed considering the size of the library. The DEG analysis was designed to reduce the batch effect resulting from the difference of the experimental time, and then fitted a generalized linear model (GLM) to statistically tested. DEG was determined based on statistically significant differences between the two biological conditions (*Eed-cKO$^{\Delta Olig2}$* and control).

To identify enriched biological themes over-represented in Eed-deficient OPC or OLs, we identified the upregulated genes with the cut-off of fold change ≥ 2 and FDR ≤ 0.05 and then analyzed Gene Ontology (GO) terms enriched in these DEG sets using DAVID ver 6.8 (Huang et al., 2009). The gene set overlapping test between the analyzed DEGs and functional categorized genes including biological process, molecular function, cellular component of GO terms. GO analysis results were also obtained with statistically significant values.

Chromatin immunoprecipitation (ChIP) and ChIP-seq analysis—To define the genome-wide binding pattern of Suz12 and Eed, the spinal cord cells were isolated from postnatal day 3 (P3) mice. Then, OPCs were purified from P7 mice using the immunopanning method and cultured *in vitro* under proliferation condition, and harvested for OPC ChIP samples. OPCs were also differentiated to OLs using differentiation medium for two days and harvested for OL ChIP samples. These cells were washed with PBS buffer, fixed in 1% formaldehyde for 10 min at room temperature, and quenched by 125 mM glycine. Cells were washed with Buffer I (0.25% Triton X-100, 10 mM EDTA, 0.5 mM

Author Manuscript Author Manuscript Author Manuscript Author Manuscript

EGTA, 10 mM HEPES, pH 7.5) and Buffer II (200 mM NaCl, 1 mM EDTA, 0.5 mM EGTA, 10 mM Tris-HCl, pH 8.0) sequentially. Then, cells were lysed with lysis buffer (0.1% SDS, 1 mM EDTA, 0.5 mM EGTA, 10 mM Tris-HCl, pH 8.0, protease inhibitor mixture) and were subjected to sonication for DNA shearing into 200–500 base pairs. Next, cell lysates were diluted 1:5 in ChIP buffer (0.1% Triton X-100, 0.1% SDS, 2 mM EDTA, 100 mM NaCl, 20 mM Tris-HCl, pH 8.0, protease inhibitor mixture) and, for immunoclearing, were incubated with IgG and protein A agarose beads for 2 hr at 4°C. Supernatant was collected after quick spin and incubated with IgG or antibodies against Suz12 or Eed together with protein A agarose beads to precipitate protein/chromatin complex overnight at 4°C. After pull-down of protein/ chromatin/antibody complex with protein A agarose beads, the beads were washed with TSE I (0.1% SDS, 1% Triton X-100, 2 mM EDTA, 20 mM Tris-HCl, pH 8.0, 150 mM NaCl), TSE II (same components as in TSE I except 500 mM NaCl), and Buffer III (0.25 M LiCl, 0.1% Nonidet P-40, 1% deoxycholate, 1 mM EDTA, 10 mM Tris-HCl, pH 8.0) sequentially for 5 min at each step. Then the beads were washed with Tris-EDTA (TE) buffer two times. Protein/chromatin complexes were eluted in elution buffer (1% SDS, 1 mM EDTA, 0.1 M NaHCO3, 10 mM Tris-HCl, pH 8.0) and decrosslinked by incubating at 65°C overnight. Eluate was incubated at 42°C for 2 hours with Proteinase K. Next, DNA was purified with Phenol/chloroform and DNA pellet was precipitated by ethanol/0.3M Sodium Acetate and dissolved in water.

Two independent ChIP-seq samples and one ChIP-seq sample were prepared with Suz12 antibody and Eed antibody, respectively. ChIP-seq DNA samples were prepared for high-throughput sequencing according to the Illumina protocol and sequenced with the Illumina HiSeq 2500 Sequencer. Reads were aligned to the mm10 reference genome using bowtie2 with default settings (Langmead and Salzberg, 2012). Subsequently, duplicated reads were removed from alignments using Picard (v.2.8.3–7) (Broad Institute, http://broadinstitute.github.io/picard/). Peak calling was performed using MACS2 (v. 2.1.1) (Zhang et al., 2008) with the following parameters: '-q 0.05 -g mm' setting a q-value threshold of 0.05 except for Suz12 replicate 2 to have a comparable number of peaks with replicate 1 by relaxing a q-value threshold to 0.1. Common peaks between two replicates were determined by presence of overlap of the position aligned to the genome reference with a tool of BEDOPS (v. 2.4.23) (Neph et al., 2012). Resulting peak sets were annotated to the genes according to close proximity of gene feature defined in TxDb.Mmusculus.UCSC.mm10.ensGene package in Bioconductor (v.3.0.0) in R (M, n.d.) using the following criteria: if a peak was enriched in a region between −2,000 bp and +2,000 bp from transcription start site, it was considered to be 'promoter'; in case of peaks that were enriched within a region between the definition of gene start and gene end, it was considered to be 'gene body'; in case of peaks that were enriched in an intergenic region, it was considered to be 'intergenic' and assigned two genes each of which is nearest in either direction.

ChIP experiments were performed in at least two independently isolated and prepared OPC and OL samples. The results were highly similar among the different sets of experiments. Primers for ChIP qPCR are listed in the Key Resources Table.

Author Manuscript Author Manuscript Author Manuscript Author Manuscript

For H3K27me3 ChIP-seq data, we reanalyzed the published H3K27me3 ChIP-seq dataset in rat OPCs (Liu et al., 2015). The reads were aligned to rat reference genome provided by UCSC (rn4) using bowtie2 (Langmead and Salzberg, 2012) and the aligned reads were further processed by filtering nonuniquely aligned reads and removing potential PCR duplicates using SAMtools (Li et al., 2009). Next, the peaks in the ChIP-seq data were called by MACS2 (Zhang et al., 2008) with q-value of 0.05. The peaks were then annotated to genes using HOMER (Heinz et al., 2010). The gene list was compared and combined with the published gene list from the same ChIP-seq dataset (Liu et al., 2015).

Chick in ovo electroporation—In ovo electroporation was performed as described (Lee et al., 2013). Briefly, chick eggs (McIntyre Farms, Portland, OR, USA) were incubated in a humidified chamber at 37°C and DNA constructs (HA-NFIA and Myc-Olig2) were injected into the lumen of chick embryonic spinal cords at HH stage 13. Electroporation was performed using a square wave electroporator (BTX) and then embryos were harvested at 4 days or 8 days after electroporation for analysis.

QUANTIFICATION AND STATISTICAL ANALYSIS

Cell count was obtained per section or area at indicated stages. At least three embryos and two sections per embryo were used for the quantification for each genotype. To quantify relative signal intensity, grayscale value for fluorescence intensity in images with 494×520 pixels were analyzed using ImageJ. The background was subtracted in each image, and the mean grayscale value was divided by the target cell number in each image to identify average expression level in single cell. Error bars represent the standard error or the standard deviation of the mean, as indicated in each figure. The significance was determined using unpaired two-tailed Student's t test or two-way ANOVA in Graphpad Prism. Significance was set at $p < 0.05$ (*, $p < 0.05$; **, $p < 0.01$; ***, $p < 0.005$).

Supplementary Material

Refer to Web version on PubMed Central for supplementary material.

ACKNOWLEDGMENTS

We are grateful to Jo Hill for help with electron micrograph analysis, Stuart Orkin for *Ezh2-flox* mice, Ben Novitch and Thomas Jessell for *Olig2-Cre* mice, Q. Richard Lu for *Olig1-Cre* mice, Ben Deneen for NFIA expression vector and antibodies, Patrizia Casaccia for sharing H3K27me3 ChIP-seq dataset, Richard Goodman and Anthony P. Barnes for critically reading this manuscript, and the Lee laboratory members for helpful discussions. This research was supported by grants from NIH/NINDS (R01NS054941, R56NS054941, and R01NS100471 to S.-K.L.; P30NS061800 to S.A.A.; and R01NS094181 and R21NS102558 to Yungki Park), NIH/NIDDK (R01DK064678 and R01DK103661 to J.W.L.), and the National Multiple Sclerosis Society (RG 5106A1); a Race to Erase MS grant (to B.E.), the Soongsil University Research Fund of 2018 (to S.K.), grants of the Korea Health Technology R&D Project through the Korea Health Industry Development Institute (KHIDI), funded by the Ministry of Health & Welfare, Republic of Korea (HI17C0447) and the Medical Research Center (MRC) (NRF-2018R1A5A2024425) through the National Research Foundation of Korea (NRF) funded by the Ministry of Science, ICT, and Future Planning (to S.L.).

REFERENCES

Aicher SA, Hermes SM, Whittier KL, and Hegarty DM (2012). Descending projections from the rostral ventromedial medulla (RVM) to trigeminal and spinal dorsal horns are morphologically and neurochemically distinct. J. Chem. Neuroanat 43, 103–111. [PubMed: 22119519]

Author Manuscript Author Manuscript Author Manuscript Author Manuscript

Boyer LA, Plath K, Zeitlinger J, Brambrink T, Medeiros LA, Lee TI, Levine SS, Wernig M, Tajonar A, Ray MK, et al. (2006). Polycomb complexes repress developmental regulators in murine embryonic stem cells. Nature 441, 349–353. [PubMed: 16625203]

Chaboub LS, Manalo JM, Lee HK, Glasgow SM, Chen F, Kawasaki Y, Akiyama T, Kuo CT, Creighton CJ, Mohila CA, and Deneen B (2016). Temporal Profiling of Astrocyte Precursors Reveals Parallel Roles for Asef during Development and after Injury. J. Neurosci 36, 11904–11917. [PubMed: 27881777]

Chen T, and Dent SY (2014). Chromatin modifiers and remodellers: regulators of cellular differentiation. Nat. Rev. Genet 15, 93–106. [PubMed: 24366184]

Clovis YM, Seo SY, Kwon JS, Rhee JC, Yeo S, Lee JW, Lee S, and Lee SK (2016). Chx10 Consolidates V2a Interneuron Identity through Two Distinct Gene Repression Modes. Cell Rep. 16, 1642–1652. [PubMed: 27477290]

Deneen B, Ho R, Lukaszewicz A, Hochstim CJ, Gronostajski RM, and Anderson DJ (2006). The transcription factor NFIA controls the onset of gliogenesis in the developing spinal cord. Neuron 52, 953–968. [PubMed: 17178400]

Dessaud E, Yang LL, Hill K, Cox B, Ulloa F, Ribeiro A, Mynett A, Novitch BG, and Briscoe J (2007). Interpretation of the sonic hedgehog morphogen gradient by a temporal adaptation mechanism. Nature 450, 717–720. [PubMed: 18046410]

Dobin A, Davis CA, Schlesinger F, Drenkow J, Zaleski C, Jha S, Batut P, Chaisson M, and Gingeras TR (2013). STAR: ultrafast universal RNA-seq aligner. Bioinformatics 29, 15–21. [PubMed: 23104886]

Dugas JC, and Emery B (2013). Purification of oligodendrocyte precursor cells from rat cortices by immunopanning. Cold Spring Harb. Protoc 2013, 745–758. [PubMed: 23906908]

Emery B, and Lu QR (2015). Transcriptional and Epigenetic Regulation of Oligodendrocyte Development and Myelination in the Central Nervous System. Cold Spring Harb. Perspect. Biol 7, a020461. [PubMed: 26134004]

Ezhkova E, Lien WH, Stokes N, Pasolli HA, Silva JM, and Fuchs E (2011). EZH1 and EZH2 cogovern histone H3K27 trimethylation and are essential for hair follicle homeostasis and wound repair. Genes Dev 25, 485–498. [PubMed: 21317239]

Fancy SP, Baranzini SE, Zhao C, Yuk DI, Irvine KA, Kaing S, Sanai N, Franklin RJ, and Rowitch DH (2009). Dysregulation of the Wnt pathway inhibits timely myelination and remyelination in the mammalian CNS. Genes Dev 23, 1571–1585. [PubMed: 19515974]

Fancy SP, Glasgow SM, Finley M, Rowitch DH, and Deneen B (2012). Evidence that nuclear factor IA inhibits repair after white matter injury. Ann. Neurol 72, 224–233. [PubMed: 22807310]

García-Alcalde F, Okonechnikov K, Carbonell J, Cruz LM, Götz S, Tarazona S, Dopazo J, Meyer TF, and Conesa A (2012). Qualimap: evaluating next-generation sequencing alignment data. Bioinformatics 28, 2678–2679. [PubMed: 22914218]

Genoud S, Lappe-Siefke C, Goebbels S, Radtke F, Aguet M, Scherer SS, Suter U, Nave KA, and Mantei N (2002). Notch1 control of oligodendrocyte differentiation in the spinal cord. J. Cell Biol 158, 709–718. [PubMed: 12186854]

Glasgow SM, Zhu W, Stolt CC, Huang TW, Chen F, LoTurco JJ, Neul JL, Wegner M, Mohila C, and Deneen B (2014). Mutual antagonism between Sox10 and NFIA regulates diversification of glial lineages and glioma subtypes. Nat. Neurosci 17, 1322–1329. [PubMed: 25151262]

Gomes WA, Mehler MF, and Kessler JA (2003). Transgenic overexpression of BMP4 increases astroglial and decreases oligodendroglial lineage commitment. Dev. Biol 255, 164–177. [PubMed: 12618141]

He L, and Lu QR (2013). Coordinated control of oligodendrocyte development by extrinsic and intrinsic signaling cues. Neurosci. Bull 29, 129–143. [PubMed: 23494530]

He F, Ge W, Martinowich K, Becker-Catania S, Coskun V, Zhu W, Wu H, Castro D, Guillemot F, Fan G, et al. (2005). A positive autoregulatory loop of Jak-STAT signaling controls the onset of astrogliogenesis. Nat. Neurosci 8, 616–625. [PubMed: 15852015]

He D, Wang J, Lu Y, Deng Y, Zhao C, Xu L, Chen Y, Hu YC, Zhou W, and Lu QR (2017). lncRNA Functional Networks in Oligodendrocytes Reveal Stage-Specific Myelination Control by an lncOL1/Suz12 Complex in the CNS. Neuron 93, 362–378. [PubMed: 28041882]

Author Manuscript Author Manuscript Author Manuscript Author Manuscript

Heinz S, Benner C, Spann N, Bertolino E, Lin YC, Laslo P, Cheng JX, Murre C, Singh H, and Glass CK (2010). Simple combinations of lineage-determining transcription factors prime cis-regulatory elements required for macrophage and B cell identities. Mol. Cell 38, 576–589. [PubMed: 20513432]

Hirabayashi Y, Suzki N, Tsuboi M, Endo TA, Toyoda T, Shinga J, Koseki H, Vidal M, and Gotoh Y (2009). Polycomb limits the neurogenic competence of neural precursor cells to promote astrogenic fate transition. Neuron 63, 600–613. [PubMed: 19755104]

Hochstim C, Deneen B, Lukaszewicz A, Zhou Q, and Anderson DJ (2008). Identification of positionally distinct astrocyte subtypes whose identities are specified by a homeodomain code. Cell 133, 510–522. [PubMed: 18455991]

Huang DW, Sherman BT, and Lempicki RA (2009). Bioinformatics enrichment tools: paths toward the comprehensive functional analysis of large gene lists. Nucleic Acids Res. 37, 1–13. [PubMed: 19033363]

Kang P, Lee HK, Glasgow SM, Finley M, Donti T, Gaber ZB, Graham BH, Foster AE, Novitch BG, Gronostajski RM, and Deneen B (2012). Sox9 and NFIA coordinate a transcriptional regulatory cascade during the initiation of gliogenesis. Neuron 74, 79–94. [PubMed: 22500632]

Kim H, Shin J, Kim S, Poling J, Park HC, and Appel B (2008). Notch-regulated oligodendrocyte specification from radial glia in the spinal cord of zebrafish embryos. Dev. Dyn 237, 2081–2089. [PubMed: 18627107]

Kondo T, and Raff M (2000a). Basic helix-loop-helix proteins and the timing of oligodendrocyte differentiation. Development 127, 2989–2998. [PubMed: 10862737]

Kondo T, and Raff M (2000b). Oligodendrocyte precursor cells reprogrammed to become multipotential CNS stem cells. Science 289, 1754–1757. [PubMed: 10976069]

Kouzarides T (2007). Chromatin modifications and their function. Cell 128, 693–705. [PubMed: 17320507]

Lachner M, Sengupta R, Schotta G, and Jenuwein T (2004). Trilogies of histone lysine methylation as epigenetic landmarks of the eukaryotic genome. Cold Spring Harb. Symp. Quant. Biol 69, 209–218. [PubMed: 16117651]

Langmead B, and Salzberg SL (2012). Fast gapped-read alignment with Bowtie 2. Nat. Methods 9, 357–359. [PubMed: 22388286]

Lee SK, and Pfaff SL (2001). Transcriptional networks regulating neuronal identity in the developing spinal cord. Nat. Neurosci 4 (Suppl), 1183–1191. [PubMed: 11687828]

Lee TI, Jenner RG, Boyer LA, Guenther MG, Levine SS, Kumar RM, Chevalier B, Johnstone SE, Cole MF, Isono K, et al. (2006). Control of developmental regulators by Polycomb in human embryonic stem cells. Cell 125, 301–313. [PubMed: 16630818]

Lee S, Shen R, Cho HH, Kwon RJ, Seo SY, Lee JW, and Lee SK (2013). STAT3 promotes motor neuron differentiation by collaborating with motor neuron-specific LIM complex. Proc. Natl. Acad. Sci. USA 110, 11445–11450. [PubMed: 23798382]

Li H, Handsaker B, Wysoker A, Fennell T, Ruan J, Homer N, Marth G, Abecasis G, and Durbin R; 1000 Genome Project Data Processing Subgroup (2009). The Sequence Alignment/Map format and SAMtools. Bioinformatics 25, 2078–2079. [PubMed: 19505943]

Liao Y, Smyth GK, and Shi W (2014). FeatureCounts: an efficient general purpose program for assigning sequence reads to genomic features. Bioinformatics 30, 923–930. [PubMed: 24227677]

Liu A, Li J, Marin-Husstege M, Kageyama R, Fan Y, Gelinas C, and Casaccia-Bonnefil P (2006). A molecular insight of Hes5-dependent inhibition of myelin gene expression: old partners and new players. EMBO J. 25, 4833–4842. [PubMed: 17006542]

Liu J, Magri L, Zhang F, Marsh NO, Albrecht S, Huynh JL, Kaur J, Kuhlmann T, Zhang W, Slesinger PA, and Casaccia P (2015). Chromatin landscape defined by repressive histone methylation during oligodendrocyte differentiation. J. Neurosci. 35, 352–365. [PubMed: 25568127]

Lock C, Hermans G, Pedotti R, Brendolan A, Schadt E, Garren H, Langer-Gould A, Strober S, Cannella B, Allard J, et al. (2002). Gene-microarray analysis of multiple sclerosis lesions yields new targets validated in autoimmune encephalomyelitis. Nat. Med 8, 500–508. [PubMed: 11984595]

Author Manuscript Author Manuscript Author Manuscript Author Manuscript

Lu QR, Yuk D, Alberta JA, Zhu Z, Pawlitzky I, Chan J, McMahon AP, Stiles CD, and Rowitch DH (2000). Sonic hedgehog-regulated oligodendrocyte lineage genes encoding bHLH proteins in the mammalian central nervous system. Neuron 25, 317–329. [PubMed: 10719888]

Lu QR, Sun T, Zhu Z, Ma N, Garcia M, Stiles CD, and Rowitch DH (2002). Common developmental requirement for Olig function indicates a motor neuron/oligodendrocyte connection. Cell 109, 75–86. [PubMed: 11955448]

Margueron R, and Reinberg D (2011). The Polycomb complex PRC2 and its mark in life. Nature 469, 343–349. [PubMed: 21248841]

Martin M (2011). Cutadapt removes adapter sequences from high-throughput sequencing reads. EMBnet J 17, 10–12.

Nakashima K, Yanagisawa M, Arakawa H, Kimura N, Hisatsune T, Kawabata M, Miyazono K, and Taga T (1999). Synergistic signaling in fetal brain by STAT3-Smad1 complex bridged by p300. Science 284, 479–482. [PubMed: 10205054]

Namihira M, Kohyama J, Semi K, Sanosaka T, Deneen B, Taga T, and Nakashima K (2009). Committed neuronal precursors confer astrocytic potential on residual neural precursor cells. Dev. Cell 16, 245–255. [PubMed: 19217426]

Neph S, Kuehn MS, Reynolds AP, Haugen E, Thurman RE, Johnson AK, Rynes E, Maurano MT, Vierstra J, Thomas S, et al. (2012). BEDOPS: high-performance genomic feature operations. Bioinformatics 28, 1919–1920. [PubMed: 22576172]

Nunes MC, Roy NS, Keyoung HM, Goodman RR, McKhann G 2nd, Jiang L, Kang J, Nedergaard M, and Goldman SA (2003). Identification and isolation of multipotential neural progenitor cells from the subcortical white matter of the adult human brain. Nat. Med 9, 439–447. [PubMed: 12627226]

Park HC, Boyce J, Shin J, and Appel B (2005). Oligodendrocyte specification in zebrafish requires notch-regulated cyclin-dependent kinase inhibitor function. J. Neurosci 25, 6836–6844. [PubMed: 16033893]

Pereira JD, Sansom SN, Smith J, Dobenecker MW, Tarakhovsky A, and Livesey FJ (2010). Ezh2, the histone methyltransferase of PRC2, regulates the balance between self-renewal and differentiation in the cerebral cortex. Proc. Natl. Acad. Sci. USA 107, 15957–15962. [PubMed: 20798045]

Petersen MA, Ryu JK, Chang KJ, Etxeberria A, Bardehle S, Mendiola AS, Kamau-Devers W, Fancy SPJ, Thor A, Bushong EA, et al. (2017). Fibrinogen Activates BMP Signaling in Oligodendrocyte Progenitor Cells and Inhibits Remyelination after Vascular Damage. Neuron 96, 1003–1012.e7. [PubMed: 29103804]

Pietersen AM, and van Lohuizen M (2008). Stem cell regulation by polycomb repressors: postponing commitment. Curr. Opin. Cell Biol 20, 201–207. [PubMed: 18291635]

Robinson MD, McCarthy DJ, and Smyth GK (2010). edgeR: a Bioconductor package for differential expression analysis of digital gene expression data. Bioinformatics 26, 139–140. [PubMed: 19910308]

Samanta J, and Kessler JA (2004). Interactions between ID and OLIG proteins mediate the inhibitory effects of BMP4 on oligodendroglial differentiation. Development 131, 4131–4142. [PubMed: 15280210]

Shen X, Liu Y, Hsu YJ, Fujiwara Y, Kim J, Mao X, Yuan GC, and Orkin SH (2008). EZH1 mediates methylation on histone H3 lysine 27 and complements EZH2 in maintaining stem cell identity and executing pluripotency. Mol. Cell 32, 491–502. [PubMed: 19026780]

Sher F, Rössler R, Brouwer N, Balasubramaniyan V, Boddeke E, and Copray S (2008). Differentiation of neural stem cells into oligodendrocytes: involvement of the polycomb group protein Ezh2. Stem Cells 26, 2875–2883. [PubMed: 18687996]

Shimizu T, Kagawa T, Wada T, Muroyama Y, Takada S, and Ikenaka K (2005). Wnt signaling controls the timing of oligodendrocyte development in the spinal cord. Dev. Biol 282, 397–410. [PubMed: 15950605]

Takebayashi H, Nabeshima Y, Yoshida S, Chisaka O, Ikenaka K, and Nabeshima Y (2002). The basic helix-loop-helix factor olig2 is essential for the development of motoneuron and oligodendrocyte lineages. Curr. Biol 12, 1157–1163. [PubMed: 12121626]

Author Manuscript Author Manuscript Author Manuscript Author Manuscript

Wang S, Sdrulla AD, diSibio G, Bush G, Nofziger D, Hicks C, Weinmaster G, and Barres BA (1998). Notch receptor activation inhibits oligodendrocyte differentiation. Neuron 21, 63–75. [PubMed: 9697852]

Xin M, Yue T, Ma Z, Wu FF, Gow A, and Lu QR (2005). Myelinogenesis and axonal recognition by oligodendrocytes in brain are uncoupled in Olig1-null mice. J. Neurosci 25, 1354–1365. [PubMed: 15703389]

Ye F, Chen Y, Hoang T, Montgomery RL, Zhao XH, Bu H, Hu T, Taketo MM, van Es JH, Clevers H, et al. (2009). HDAC1 and HDAC2 regulate oligodendrocyte differentiation by disrupting the beta-catenin-TCF interaction. Nat. Neurosci 12, 829–838. [PubMed: 19503085]

Yoo KH, Oh S, Kang K, Hensel T, Robinson GW, and Hennighausen L (2015). Loss of EZH2 results in precocious mammary gland development and activation of STAT5-dependent genes. Nucleic Acids Res 43, 8774–8789. [PubMed: 26250110]

Yu M, Riva L, Xie H, Schindler Y, Moran TB, Cheng Y, Yu D, Hardison R, Weiss MJ, Orkin SH, et al. (2009). Insights into GATA-1-mediated gene activation versus repression via genome-wide chromatin occupancy analysis. Mol. Cell 36, 682–695. [PubMed: 19941827]

Yu Y, Chen Y, Kim B, Wang H, Zhao C, He X, Liu L, Liu W, Wu LM, Mao M, et al. (2013). Olig2 targets chromatin remodelers to enhancers to initiate oligodendrocyte differentiation. Cell 152, 248–261. [PubMed: 23332759]

Zhang Y, Liu T, Meyer CA, Eeckhoute J, Johnson DS, Bernstein BE, Nusbaum C, Myers RM, Brown M, Li W, and Liu XS (2008). Model-based analysis of ChIP-Seq (MACS). Genome Biol 9, R137. [PubMed: 18798982]

Zhou Q, and Anderson DJ (2002). The bHLH transcription factors OLIG2 and OLIG1 couple neuronal and glial subtype specification. Cell 109, 61–73. [PubMed: 11955447]

Zhou Q, Wang S, and Anderson DJ (2000). Identification of a novel family of oligodendrocyte lineage-specific basic helix-loop-helix transcription factors. Neuron 25, 331–343. [PubMed: 10719889]

Zhu X, Zuo H, Maher BJ, Serwanski DR, LoTurco JJ, Lu QR, and Nishiyama A (2012). Olig2-dependent developmental fate switch of NG2 cells. Development 139, 2299–2307. [PubMed: 22627280]

Author Manuscript Author Manuscript Author Manuscript Author Manuscript

Highlights

- PRC2 null oligodendrocyte (OL) lineage cells fail to differentiate to OL
- PRC2 null OL lineage cells aberrantly upregulate Notch and Wnt pathway genes
- The inhibition of Notch and Wnt restores OL differentiation in PRC2 null OL cells
- The Notch inhibition blocks aberrant astrocytic gene induction in PRC2 null OL cells

Author Manuscript Author Manuscript Author Manuscript Author Manuscript

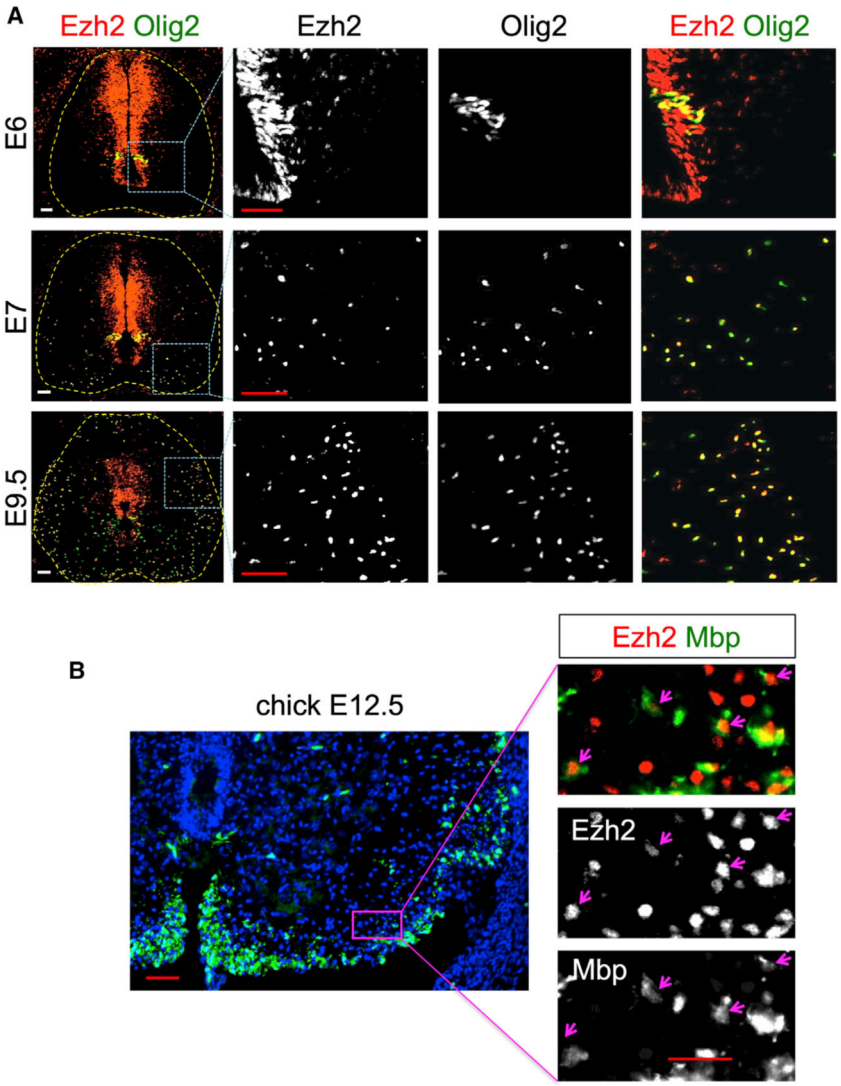

Figure 1. Ezh2 Is Expressed in the OL Lineage in the Developing Spinal Cord

Immunohistochemical analyses with Ezh2 and Olig2 antibodies (A) or Ezh2 and Mbp antibodies (B) in the spinal cord of chick embryos at E9.5–E12.5. Only the ventro-lateral region of one side of the spinal cord is shown in (B). Scale bars, 50 μm (A), 50 μm (left panel in B), or 20 μm (magnified images in B).

Author Manuscript Author Manuscript Author Manuscript Author Manuscript

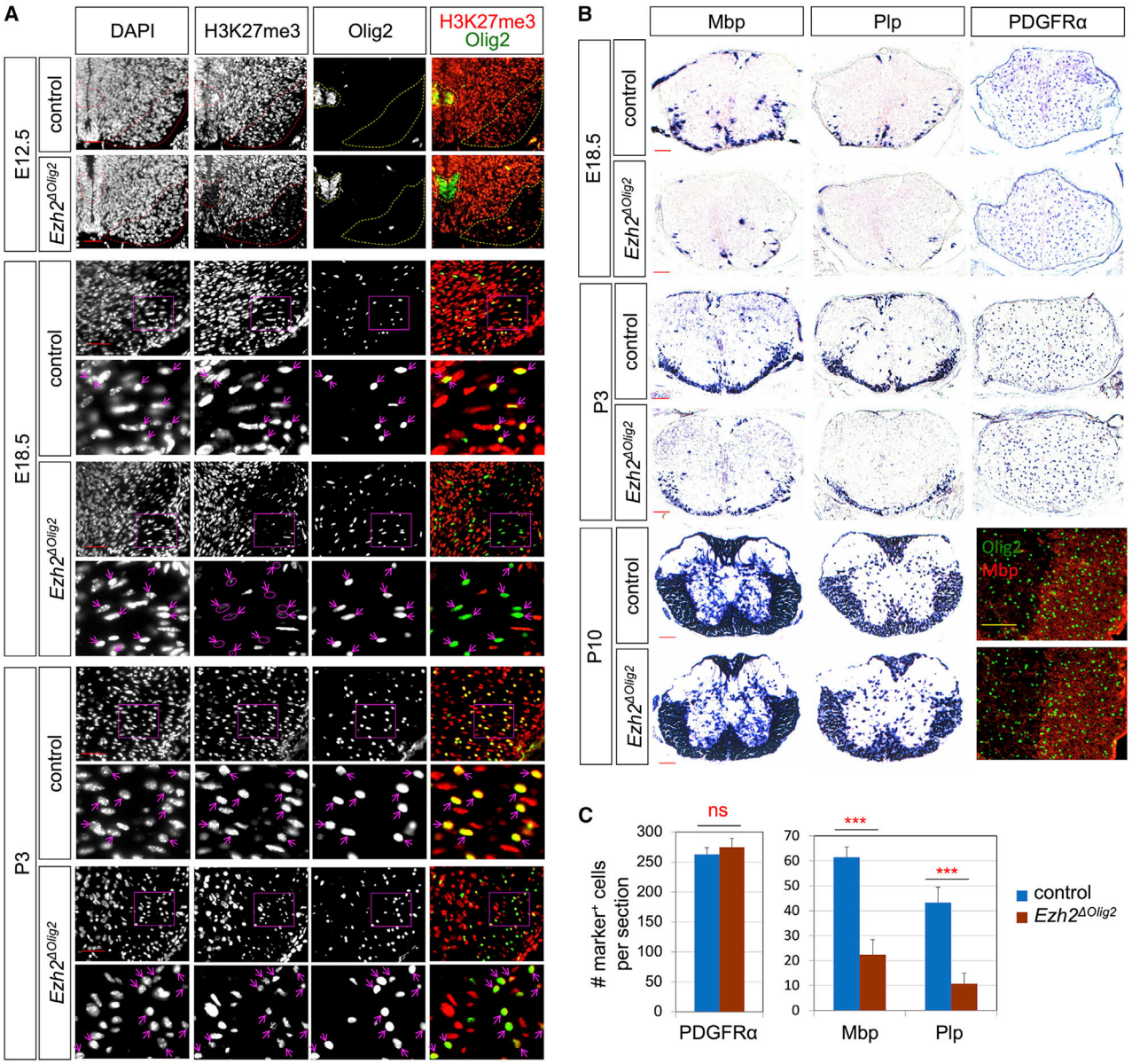

Figure 2. Ezh2 Is Needed for Generation of the H3K27me3 Repressive Mark in the OL Lineage and for OL Differentiation, but Not for OPC Production, in the Embryonic CNS

(A) Immunohistochemical analyses of the spinal cord of *Ezh2-Cko*$^{\Delta Olig2}$ (*Ezh2*$^{\Delta Olig2}$) and their littermate control mice with Olig2 and H3K27me3 antibodies. H3K27me3 levels were markedly reduced in cells in pMN and motor neuron areas (dotted circles) in *Ezh2*$^{\Delta Olig2}$ mice at E12.5. The H3K27me3 mark remained absent from OPCs and OLs at E18.5 and partially recovered at P3 in *Ezh2*$^{\Delta Olig2}$ mice. Only the ventro-lateral regions of one side of the spinal cord are shown. Scale bars, 50 μm.

(B) *In situ* hybridization analyses with antisense RNA probes for Mbp, Plp, and PDGFRα and immunohistochemical analyses with Mbp and Olig2 antibodies. In *Ezh2*$^{\Delta Olig2}$ mice, Mbp^{+} and Plp1^{+} OLs, but not PDGFRα^{+} OPCs, were drastically reduced in the spinal cord at E18.5 but restored to levels comparable to those of control mice at P10. Scale bars, 100 μm.

Author Manuscript Author Manuscript Author Manuscript Author Manuscript

(C) Quantification of the number of cells expressing PDGFRα, Mbp, or Plp in an 18 μm section of the spinal cord of E18.5 mice. n = 3 mice/genotype, ≥2 slices/mouse. The error bars represent the standard deviation of the mean. ***$p < 0.005$; ns, nonsignificant; two-tailed Student's t test.

Author Manuscript Author Manuscript Author Manuscript Author Manuscript

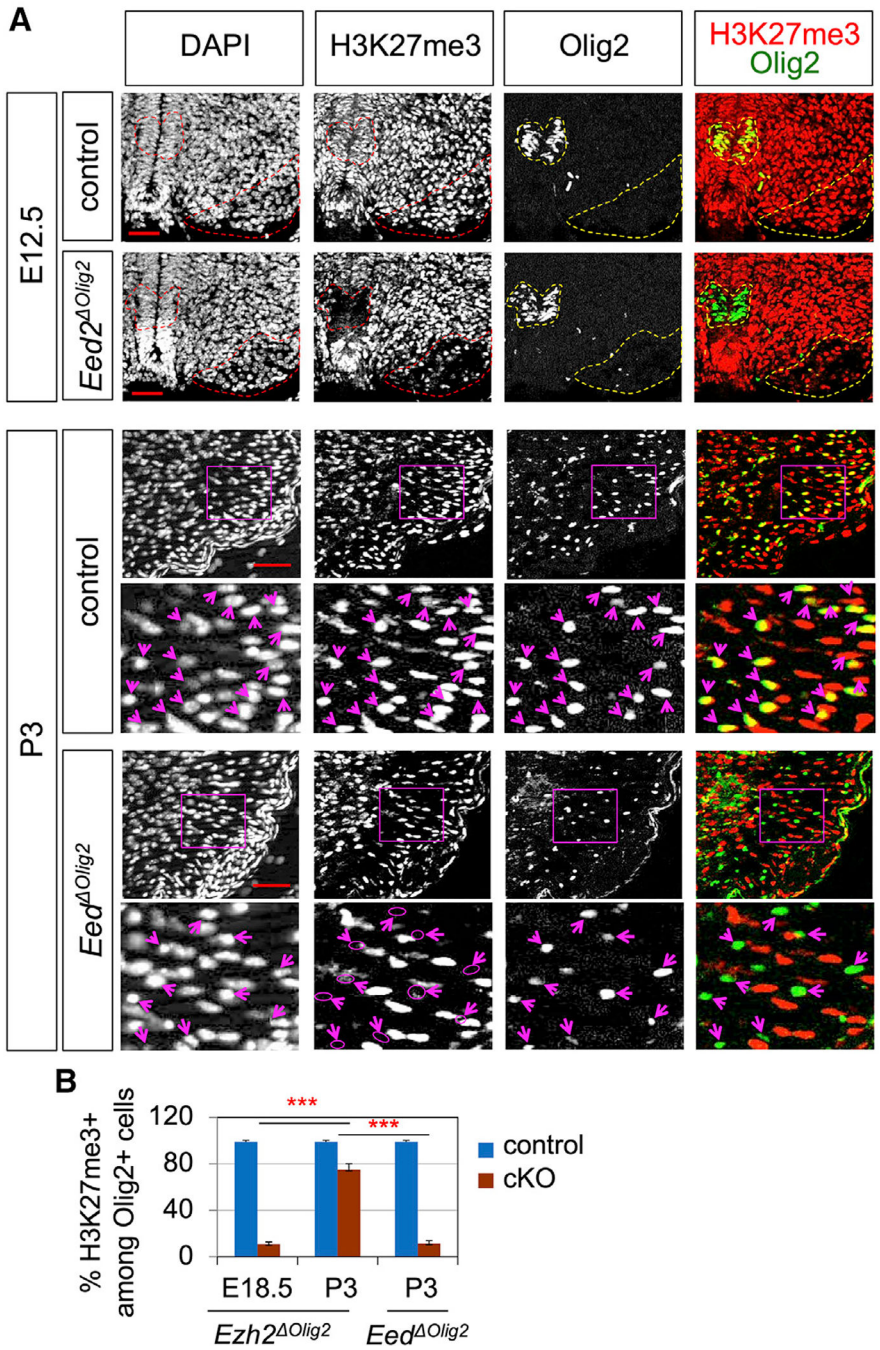

Figure 3. PRC2 Is Required for OL Differentiation and Myelination

(A) Immunohistochemical analyses of the spinal cord of *Eed-cKO*$^{\Delta Olig2}$ (*Eed*$^{-\Delta}$*Olig2*) and their littermate control mice with Olig2 and H3K27me3 antibodies. H3K27me3 levels drastically decreased in cells in pMN and MN areas (dotted circles) in E12.5 *Eed*$^{\Delta Olig2}$ mice. The H3K27me3 mark was also eliminated from OPCs and OLs in P3 *Eed*$^{\Delta Olig2}$ mice. Only the ventro-lateral regions of one side of the spinal cord are shown. Scale bars, 50 μm.

(B) Quantification of the percentage of H3K27me3^{+} cells among Olig2^{+} cells in the ventro-lateral region of the mouse spinal cord at E18.5 or P3. n = 4 mice/genotype, ≥2 slices/

Author Manuscript Author Manuscript Author Manuscript Author Manuscript

mouse. The error bars represent the standard deviation of the mean. ***$p < 0.005$, two-way ANOVA test. At P3, the H3K27me3 mark in $Olig2^+$ cells was substantially recovered in *Ezh2-cKO*$^{\Delta Olig2}$ (*Ezh2*$^{\Delta Olig2}$) mice, whereas it remained low in *Eed*$^{\Delta Olig2}$ mice.

(C) *In situ* hybridization analyses with antisense RNA probes for Mbp, Plp, and PDGFRα and immunohistochemical analyses with Mbp and Olig2 antibodies. *Eed*$^{\Delta Olig2}$ mice exhibited a loss of Mbp^+ and $Plp1^+$ OLs, but not $PDGFR\alpha^+$ OPCs, in the spinal cord at P3 and P10. Scale bars, 100 μm.

(D) Electron micrograph analysis of spinal cord and optic nerves at P13. Scale bars, 1 μm. *Eed*$^{\Delta Olig2}$ mice showed deficiency of axonal myelination.

Author Manuscript Author Manuscript Author Manuscript Author Manuscript

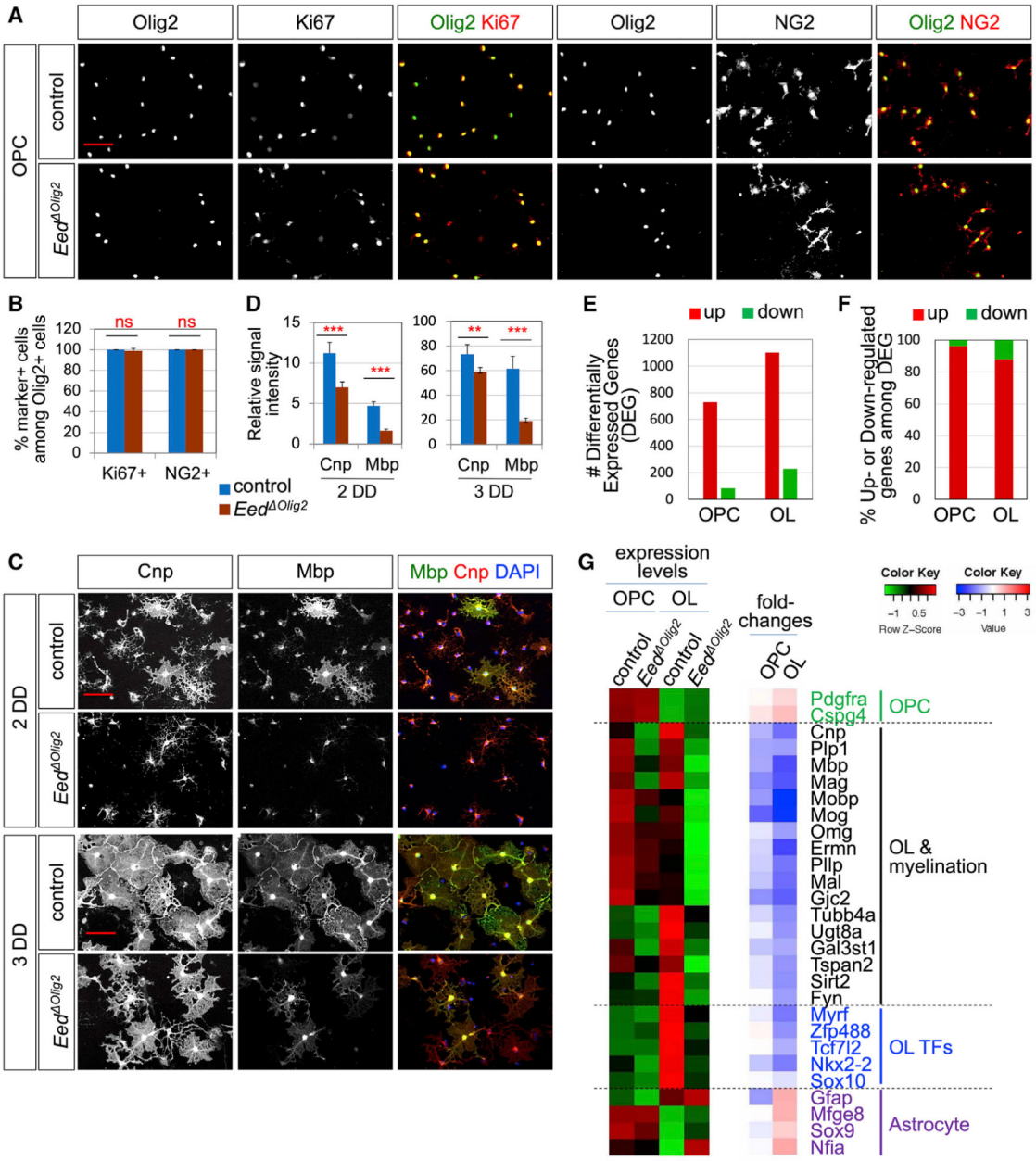

Figure 4. PRC2-Deficient OPCs Display Severe Defects in OL Differentiation

(A–D) Immunostaining analyses of cultures of OPCs isolated from *Eed-cKO*$^{\Delta Olig2}$ (*Eed*$^{\Delta Olig2}$) and control mice in proliferative (A and B) or differentiation (C and D) conditions. Scale bars, 50 μm in (A) and (C). (B) Quantification of the percentage of Ki67^{+} or NG2^{+} cells among Olig2^{+} cells in OPCs under the proliferative condition, as shown in (A). (D) Quantification of the fluorescence signal intensity for Cnp or Mbp staining under the differentiation condition, as shown in (C). (B and D) n = 3 for control and n = 4 for *Eed*$^{\Delta Olig2}$ mice, ≥2 slices/mouse. The error bars represent the standard deviation of the mean. ***p < 0.005; ns, nonsignificant; two-tailed Student's t test.

(E and F) RNA-seq analyses revealed differentially expressed genes (DEGs) in Eed-deficient OPCs or OLs compared with control OPCs or OLs. The upregulated and downregulated

Author Manuscript Author Manuscript Author Manuscript Author Manuscript

genes are shown in red and green, respectively. (E) The number of DEGs in either OPCs or OLs. (F) The percentage of up- or downregulated genes over the total DEGs in either OPCs or OLs.

(G) RNA-seq expression analyses of OPC, OL, and astrocytic gene expression in acutely isolated OPCs or OLs differentiated for 2 days (2 DD) from *Eed-cKO*$^{\Delta Olig2}$ (*Eed*$^{\Delta Olig2}$) and control mice. The heatmap on the left shows expression levels of each gene in OPCs or OLs of *Eed*$^{\Delta Olig2}$ and control mice. The heatmap on the right shows fold changes of each gene expression level in *Eed*$^{\Delta Olig2}$ samples relative to control samples. In this heatmap, blue and red represent down- and upregulation, respectively, in *Eed*$^{\Delta Olig2}$ cells compared with control cells. In Eed null OL lineage cells, OL and myelination genes were markedly reduced, whereas astrocytic genes were aberrantly increased.

Author Manuscript Author Manuscript Author Manuscript Author Manuscript

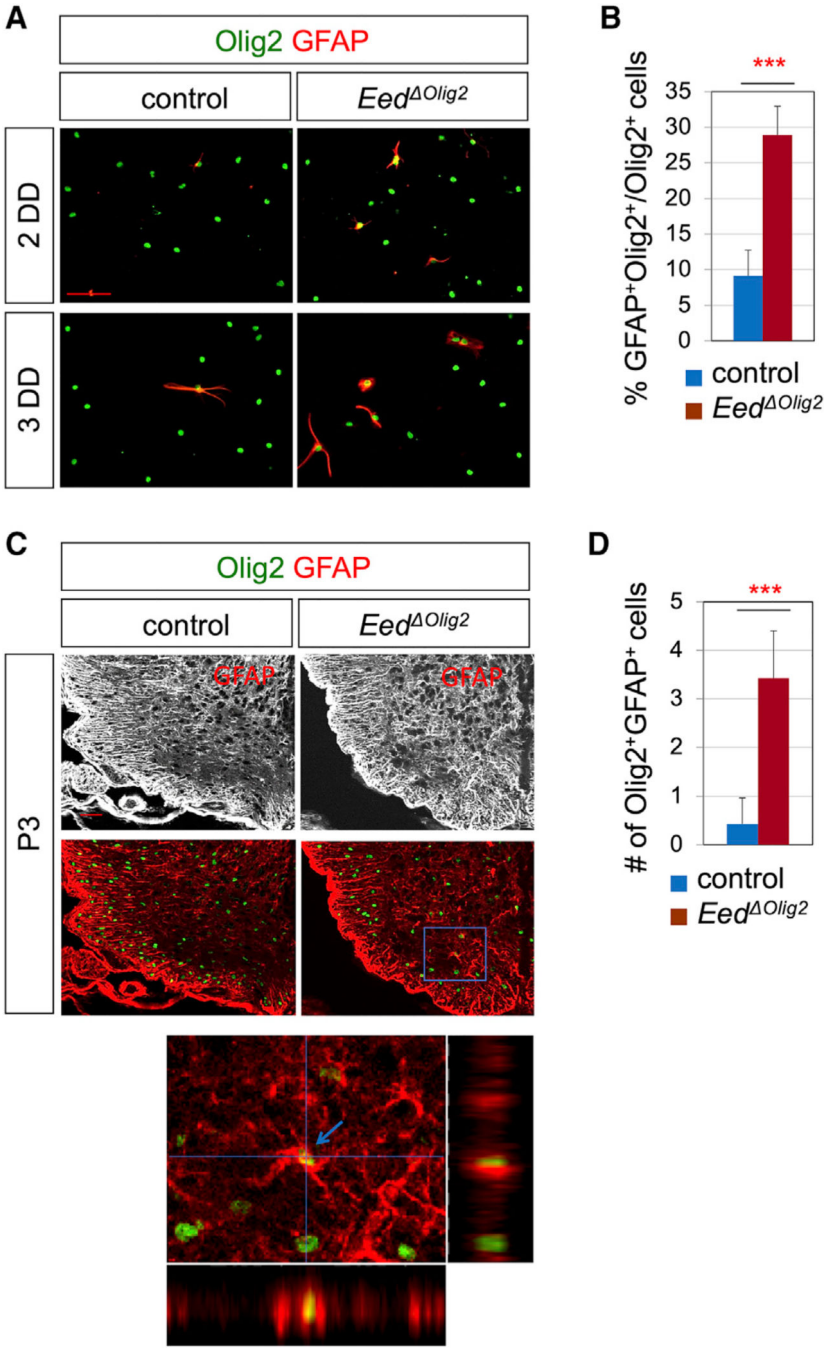

Figure 5. Astrocyte Gene Program Was Aberrantly Induced in the Eed-Deficient OL Lineage

(A and B) Immunostaining analyses of cultures of OPCs from *Eed-cKO*$^{\Delta Olig2}$ (*Eed*$^{\Delta Olig2}$) and control mice under the differentiation condition for 2 or 3 days. Scale bar, 50 μm. (B) Quantification of the percentage of GFAP/Olig2 double-positive cells among Olig2^{+} cells in 3 DD samples. n = 3 mice/genotype, ≥3 slices/mouse. The error bars represent the standard deviation of the mean. ***p < 0.005, two-tailed Student's t test.

(C and D) Immunohistochemical analyses of the spinal cord of *Eed*$^{\Delta Olig2}$ and control mice at P3. Scale bar, 50 μm. (D) Quantification of the number of GFAP/Olig2 double-positive cells

in the gray matter of the ventro-lateral region of one side of 18-μm-thick spinal cord sections. n = 3 mice/genotype, ≥3 slices/mouse. The error bars represent the standard deviation of the mean. ***p < 0.005, two-tailed Student's t test.

Author Manuscript Author Manuscript Author Manuscript Author Manuscript

Author Manuscript Author Manuscript Author Manuscript Author Manuscript

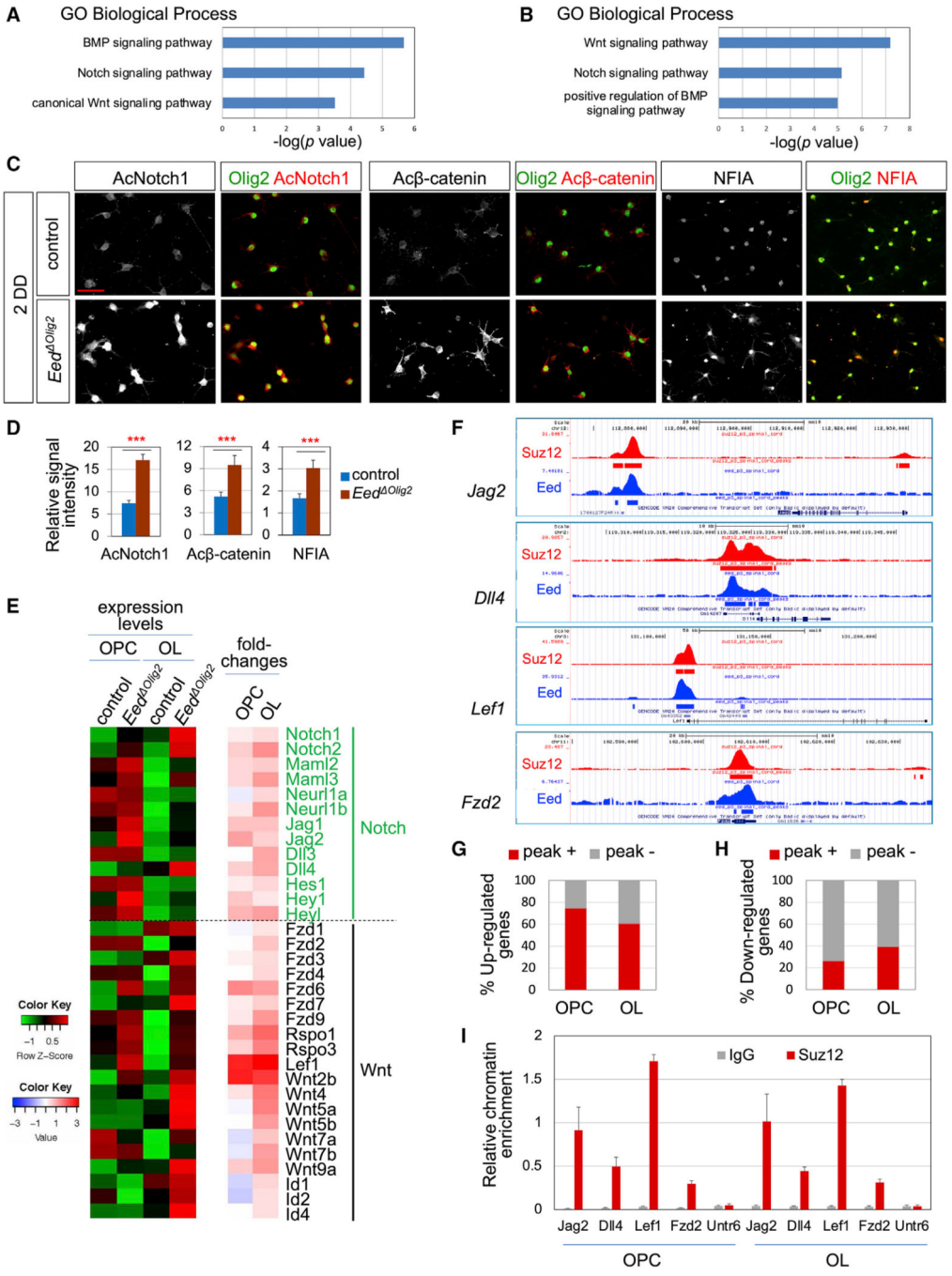

Figure 6. PRC2 Suppresses Notch and Wnt Pathway Genes

(A and B) GO analyses of genes upregulated in Eed-deficient OPCs (A) or OLs (B) from RNA-seq. GO terms of Wnt, Notch, and BMP signaling pathways are enriched in both datasets.

(C and D) Immunostaining analyses of iOLs from *Eed-cKO*$^{\Delta Olig2}$ (*Eed*$^{\Delta Olig2}$) and control mice at 2 DD with antibodies against active Notch1 (AcNotch1), active β-catenin (Acβ-catenin), and NFIA. AcNotch1, Acβ-catenin, and NFIA levels increased in Eed-deficient iOLs compared with control iOLs. Scale bar, 50 μm. (D) Quantification of the fluorescence

Author Manuscript Author Manuscript Author Manuscript Author Manuscript

signal intensity for the samples shown in (C). n = 3 for control and n = 4 for *Eed*$^{\Delta Olig2}$ mice. The error bars represent the standard deviation of the mean. ***p < 0.005, two-tailed Student's t test.

(E) RNA-seq expression analyses of Notch and Wnt signaling genes in acutely isolated OPCs or 2 DD OLs from *Eed*$^{\Delta Olig2}$ and control mice. The heatmap on the left shows expression levels of each gene in OPCs or OLs of *Eed*$^{\Delta Olig2}$ and control mice. The heatmap on the right shows fold changes of each gene expression level in *Eed*$^{\Delta Olig2}$ samples relative to control samples. In this heatmap, blue and red represent down- and upregulation, respectively, in *Eed*$^{\Delta Olig2}$ cells compared with control cells. In Eed null OL lineage cells, many Notch and Wnt pathway genes were significantly upregulated.

(F) Genome browser view of ChIP-seq peaks for Suz12 (red) and Eed (blue) on the representative target genes. Both Suz12 and Eed were recruited to the selected target genes.

(G and H) Integrative analyses of RNA-seq and ChIP-seq datasets. Most upregulated genes were annotated to Suz12-bound peaks, whereas most downregulated genes were not. (G) Percentage of upregulated genes in Eed null OPCs or OLs, which were either annotated (red, peak +) or not annotated (gray, peak −) to Suz12-bound ChIP-seq peaks. (H) Percentage of downregulated genes in Eed null OPCs or OLs, which were either annotated (red, peak +) or not annotated (gray, peak −) to Suz12-bound ChIP-seq peaks

(I) ChIP analyses with Suz12 antibody or immunoglobulin G (IgG) control in OPCs or 2 DD OLs, which were purified from wild-type mice and cultured *in vitro*. Suz12 bound to the *Jag2, Dll4, Lef1*, and *Fzd2* genes in OPCs and OLs, but not to *Untr6*, a negative control gene. The error bars represent the standard deviation of the mean.

Author Manuscript Author Manuscript Author Manuscript Author Manuscript

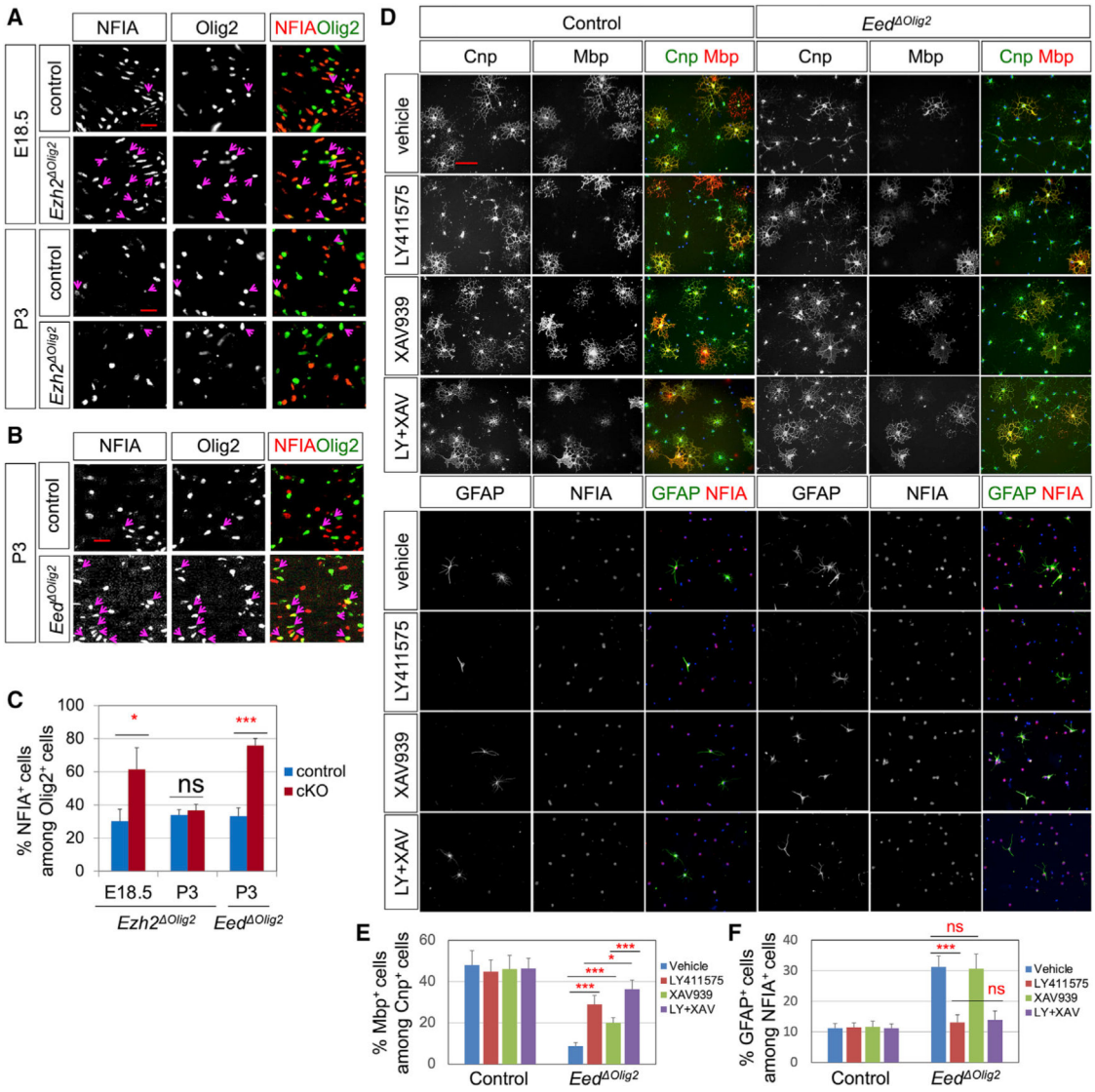

Figure 7. The Notch Pathway Is a Major Repressive Target of PRC2 in Promoting OL Differentiation and Suppressing the Astrocytic Fate

(A–C) Immunohistochemical analyses of the spinal cord of *Ezh2-cKO*$^{\Delta Olig2}$ (*Ezh2*$^{\Delta Olig2}$, A), *Eed-cKO*$^{\Delta Olig2}$ (*Eed*$^{\Delta Olig2}$, B), and their littermate control mice with NFIA and Olig2 antibodies. The percentage of NFIA/Olig2 double-positive cells among Olig2^{+} cells in *Ezh2*$^{\Delta Olig2}$, *Eed*$^{\Delta Olig2}$, and their littermate control mice at E18.5 or P3 was quantified in (C). The number of NFIA-expressing Olig2^{+} OPCs (arrows) in E18.5 *Ezh2*$^{\Delta Olig2}$ and P3 *Eed*$^{\Delta Olig2}$ mice was substantially more than that in control mice, but it was similar between P3 *Ezh2*$^{\Delta Olig2}$ mice and their littermate control mice. Scale bars, 20 μm. n = 3 mice/genotype, ≥2 slices/mouse. The error bars represent the standard deviation of the mean. *p < 0.05; ***p < 0.005; ns, nonsignificant; two-way ANOVA test.

(D–F) Immunostaining analyses of cultures of OPCs that were purified from *Eed-cKO*$^{\Delta Olig2}$ (*Eed*$^{\Delta Olig2}$) or control mice and differentiated for 3 days in the presence of the Notch inhibitor LY411575 alone, the Wnt inhibitor XAV939 alone, the combination of both inhibitors, or vehicle. Scale bar, 50 μm. (E and F) Quantification of the immunostaining

Author Manuscript Author Manuscript Author Manuscript Author Manuscript

results in (D). n = 3 for control and n = 4 for *Eed*$^{\Delta Olig2}$ mice. The error bars represent the standard deviation of the mean. *p < 0.05; ***p < 0.005; ns, nonsignificant; two-way ANOVA test. The Notch inhibitor and Wnt inhibitor significantly increased OL differentiation in the Eed null OL lineage, which was augmented by co-treatment of both inhibitors. In contrast, Notch inhibition suppressed the aberrantly increased GFPA^{+} cells in Eed-deficient OL lineage cells, but Wnt inhibition did not.

Author Manuscript Author Manuscript Author Manuscript Author Manuscript

KEY RESOURCES TABLE

REAGENT or RESOURCE	SOURCE	IDENTIFIER
Antibodies		
Goat anti-Olig2	R&D Systems	Cat#AF2418; RRID: AB_2157554
Rabbit anti-Olig2	Millipore	Cat#AB9610; RRID: AB_570666
Rabbit anti-Ezh2	Cell Signal Technology	Cat# 12408; RRID: AB_2797901
Mouse anti-Ezh2	Cell Signal Technology	Cat# 3147; RRID: AB_10694383
Rabbit anti- Histone H3K27me3	Millipore	Cat# 07-449; RRID: AB_310624
Rat anti-MBP	Millipore	Cat# MAB386; RRID: AB_94975
Mouse anti-CNP	Millipore	Cat# MAB326R; RRID: AB_11210906
Rabbit anti-NG2	Millipore	Cat# AB5320; RRID: AB_11213678
Rabbit anti-Ki67	Abcam	Cat# ab15580; RRID: AB_443209
Rat anti-Brdu	Abcam	Cat# ab6326; RRID: AB_305426
Rabbit anti-Activated Notch1	Abcam	Cat# ab8925; RRID: AB_306863
Rabbit anti-Non-phospho (Active) β-Catenin	Cell Signal Technology	Cat# 19807; RRID: AB_2650576
Rabbit anti-p-Smad1/5/8	Cell Signal Technology	Cat# 13820; RRID: AB_2493181
Rabbit anti-p-stat3	Cell Signal Technology	Cat# 9145; RRID: AB_2491009
Mouse anti-GFAP	Millipore	Cat# MAB360; RRID: AB_11212597
Rabbit anti-NFIA	Dr. Benjamin Deneen	Deneen et al., 2006
Mouse anti-EED	Millipore	Cat# 17-663; RRID: AB_10615638
Rabbit anti-Suz12	Cell Signal Technology	Cat# 3737; RRID: AB_2196850
Mouse anti-Ran-2	ATCC	Cat# TIB-119; RRID: CVCL_G149
Mouse anti-GalC	Millipore	Cat# MAB342; RRID: AB_94857
Mouse anti-O4	Millipore	Cat# MAB345; RRID: AB_11213138
Chemicals, Peptides, and Recombinant Proteins		
LY411575	Selleck Chemicals	S2714; CAS: 209984-57-6
XAV-939	Selleck Chemicals	S1180; CAS: 284028-89-3
Deposited Data		
RNA-seq & ChIP-seq data	This paper	GEO: GSE130628
Experimental Models: Organisms/ Strains		
Mouse: Ezh2fl/fl: B6;129S1-*Ezh2*^{tm2Sho}/J	Dr. Stuart Orkin	Shen et al., 2008
Mouse: EEDfl/fl: B6;129S1-*Eed*^{tm1Sho}/J	The Jackson Laboratory	RRID: IMSR_JAX: 022727
Mouse: Olig2-Cre: B6.129-*Olig2*$^{tm1.1(cre)Wdr}$/J	Dr. Bennett G. Novitch	Dessaud et al., 2007
Mouse: Olig1-Cre: B6;129S4-*Olig1*$^{tm1(cre)Rth}$/J	Dr. Q. Richard Lu	Xin et al., 2005
Oligonucleotides		

Author Manuscript Author Manuscript Author Manuscript Author Manuscript

REAGENT or RESOURCE	SOURCE	IDENTIFIER
ChIP-qPCR mouse Untr6	This paper	Forward: 5′- GCATGAACCACCATACCTAGAC Reverse: 5′- TCAGAGGGTGGACATTGGTATT
ChIP-qPCR mouse Jag2	This paper	Forward: 5′- TCACCTTGGCCTGGTACTC Reverse: 5′- CTGCGCTGCCTTATTTTTAGG
ChIP-qPCR mouse Dll4	This paper	Forward: 5′- GATCCAAATCCCCTGGTCCT Reverse: 5′- AGGATAGGAGGGTAGCCCAG
ChIP-qPCR mouse Lef1	This paper	Forward: 5′- TTCGCTCCCAAACTAAACCC Reverse: 5′- GGAGGTTGGCTGTAGTAGGT
ChIP-qPCR mouse Fzd2	This paper	Forward: 5′- TTCTGCCAGCCCATCTCC Reverse: 5′- CGCGTACATGGAGCACAG
Recombinant DNA		
pBS-mouse Ezh2(1-867bp)	This paper	For ISH
pBS-mouse Ezh1(1-867bp)	This paper	For ISH
RCAS-myc-chick Olig2	Dr. Benjamin Deneen	Deneen et al., 2006
RCAS-HA-mouse NFIA	Dr. Benjamin Deneen	Deneen et al., 2006
Software and Algorithms		
ImageJ	https://imagej.nih.gov/ij/	Java 1.8.0_112
GraphPad Prism	https://www.graphpad.com/scientific-software/prism/	Version 5.0f
STAR	Dobin et al., 2013	Ver 2.6.0
QualiMap	García-Alcalde et al., 2012	Ver 2.2.1
FeatureCounts	Liao et al., 2014	Ver 1.6.2
EdgeR	Robinson et al., 2010	N/A
DAVID	Huang et al., 2009	Ver 6.8
Bowtie2	Langmead and Salzberg, 2012	N/A
Picard	http://broadinstitute.github.io/picard/	V.2.8.3-7
MACS2	Zhang et al., 2008	V. 2.1.1
BEDOPS	Neph et al., 2012	V. 2.4.23